Mantle Dynamics of the Central Atlantic Magmatic Province (CAMP): Constraints from Platinum Group, Gold and Lithophile Elements in Flood Basalts of Morocco

Christian Tegner (1)*

Sandra A. T. Michelis (1)

Iain McDonald (2)

Eric L. Brown (1)

Nasrrddine Youbi (3, 4)

Sara Callegaro (5)

Sofie Lindström (6)

Andrea Marzoli (7)

1, Centre of Earth System Petrology (ESP), Department of Geoscience, Aarhus University, Denmark

2, School of Earth & Ocean Sciences, Cardiff University, U.K.

3, Department of Geology, Cadi Ayyad University, Marrakesh, Morocco

4, Instituto Dom Luiz, Faculdade de Ciências, Universidade de Lisboa, Lisboa, Portugal

5, Centre for Earth Evolution Dynamics (CEED), University of Oslo, Norway

6, Geological Survey of Denmark and Greenland (GEUS), Copenhagen, Denmark

7, Department of Geoscience, University of Padova, Italy

*Corresponding author: email christian.tegner@geo.au.dk; telephone +45 51928201

ABSTRACT

Mantle melting dynamics of the Central Atlantic Magmatic Province (CAMP) are constrained from new platinum group element (PGE), rare earth element (REE), and high field strength element (HFSE) data and geochemical modelling of flood basalts in Morocco. The PGE are enriched similarly to flood basalts of other large igneous provinces. The magmas did not experience sulphide saturation during fractionation and were therefore fertile. The CAMP province is thus prospective for PGE and Gold mineralisation. The Pt/Pd ratio of the Moroccan lavas indicates that they originated by partial melting of the asthenospheric mantle, not the subcontinental lithospheric mantle. Mantle melting modelling of PGE, REE and HFSE suggests: (1) that the mantle source for all the lavas was dominated by primitive mantle and invariably included a small proportion of recycled continental crust (<8%); (2) the mantle potential temperature was moderately elevated (c. 1430°C) relative to ambient mantle; (3) intra-lava unit compositional variations are likely a combined result of variable amounts of crust in the mantle source (heterogeneous source) and fractional crystallisation; (4) mantle melting initially took place at depths between c. 110 km and c. 55 km and became shallower with time (c. 110 km to c. 32 km depth); and (5) the melting region appears to have changed from triangular to columnar with time. These results are best explained by melting of asthenospheric mantle that was mixed with continental sediments during the assembly of Pangaea, then heated and further mixed by convection while insulated under the Pangaea supercontinent, and subsequently melted in multiple continental rift systems associated with the breakup of Pangaea. Most likely the CAMP volcanism was triggered by the arrival of a mantle plume, although plume material apparently was not contributing directly (chemically) to the magmas in Morocco, nor to many other areas of CAMP.

KEY WORDS: Platinum Group Elements; flood basalt; mantle melting modelling; large igneous province; geodynamics

INTRODUCTION

The Central Atlantic Magmatic Province (CAMP) is the largest known large igneous province (LIP) on Earth in terms of area (>10 million km^2) and is associated with the breakup of the Pangaea supercontinent (e.g. Marzoli *et al*., 2018). Eroded remnants of flood basalts and intrusions are preserved on four continents (Africa, Europe, North and South America) and once made up >3 million km^3 (Fig. 1). Although the thicknesses of the volcanic units of CAMP are modest (up to 0.4 km thick) compared to other LIPs, lavas and dykes of the dominant low-Ti magma type have been correlated across all four continents (Marzoli *et al*., 2018). Recent U-Pb chronology suggests that a large portion of the magmas were emplaced across all four continents within a few hundred thousand years c. 201.5 million years ago and can be shown to correlate with the end-Triassic mass extinction, suggesting a causal relationship between the two events (Blackburn *et al*., 2013; Davies *et al*., 2017). While the correlation of volcanism and environmental perturbations has become remarkably detailed due to recent research foci (e.g. Dal Corso *et al*., 2014; Lindström *et al*., 2015, 2017; Heimdal *et al*., 2018; Panfili *et al*., 2019), understanding the nature of the mantle sources and the mantle melting dynamics that produced the CAMP remains incomplete. Some workers have argued for the arrival of a mantle plume that caused extensive mantle melting and volcanism across the four continents prior to continental breakup (Morgan, 1983; Hill, 1991; Wilson, 1997, Oyarzun *et al*., 1997; Ruiz-Martinez *et al*., 2012). In this model (Sleep, 1997) hot, upwelling plume mantle rapidly spreads out laterally below the continental lithosphere, ascends and melts under the thinned lithosphere associated with the incipient rift zones of the Central Atlantic to produce the CAMP. The plume model is supported by 201 Ma plate reconstructions showing that CAMP was located vertically above a plume generation zone at the edge of a Large Low Shear-wave Velocity Province (LLSVP) at the core-mantle boundary (Torsvik *et al*., 2006; Ruiz-Martinez *et al*., 2012; Svensen *et al.,* 2018). There are, however, several challenges to this model, such as a lack of a subsequent plume track (McHone, 2000). Another challenge is that the compositions of the CAMP lavas are basaltic, but carry a strong continental signature that is different from normal mantle plume magmas and more akin to arc magmas (Puffer, 2001). However, as discussed below, Os isotope compositions have demonstrated that the crustal signature cannot result from simple crustal contamination alone, but must be an inherited feature of the mantle source (Callegaro *et al*., 2013, 2014a, 2017; Merle *et al*., 2011, 2014; Marzoli *et al*., in revision). It has therefore been argued that continental sediments were translated to the mantle source via subduction zone processes associated

with the assembly of the Pangaea supercontinent (Pegram, 1990; Puffer, 2001; Dorais & Tubrett, 2008; Callegaro *et al*., 2013, 2014; Merle *et al*., 2011, 2014a; Whalen *et al*., 2015; Shellnutt *et al*., 2018). Several workers therefore argue that the CAMP magmas were produced in the subcontinental lithospheric mantle (SCLM) (Pegram, 1990; Puffer, 2001; Cebria *et al*., 2003; Dorais & Tubrett, 2008; Martins *et al*., 2008), whereas others argue that the CAMP magmas were derived mainly from the shallow asthenospheric mantle that was mixed with continental sediments during the assembly of Pangaea (Callegaro *et al*., 2013, 2014a; Merle *et al*., 2011, 2014; Whalen *et al*., 2015; Marzoli *et al*., 2018). It has also been suggested that the mantle source of the CAMP volcanism changed with time from enriched lithosphere to depleted asthenosphere (Marzoli *et al*., 2006). Notably, most studies of the mantle sources for the CAMP have been based on samples from Eastern North America, perhaps because this region displays the highest density of dykes including the most primitive CAMP basalts (Callegaro *et al*., 2013) or because southeast North America was considered by several authors as the site of the first mantle-plume impingement (e.g. De Boer & Snider, 1979; Hill, 1991; May, 1971; Wilson, 1997). However, the most complete CAMP lava succession and related intrusives crop out in Morocco and are described in detail in a companion paper including new Sr-Nd-Pb-Os isotope data (Marzoli *et al*., in revision).

To throw new light on the mantle sources and the melting dynamics of the CAMP we report here on the platinum group elements (PGE), gold (Au), and copper (Cu), together with the lithophile major and trace element compositions of CAMP basalts from Morocco. While the lithophile element composition of mantle melts is controlled by the silicate phases in the mantle, the PGE and Au concentrations are essentially controlled by mantle sulphide phases (Keays, 1995; Carlson, 2005) due to the extremely high partition coefficients for the PGEs into sulphide (D-values in the order of 10^5-10^6, Mungall & Brenan, 2014). Moreover, some of the PGEs (Os, Ir and Ru; the IPGEs) are compatible in mantle silicates, in alloys, and in platinum group minerals associated with chromite and/or olivine (Mungall & Brenan, 2014; Barnes *et al*., 2015; Arguin *et al*., 2016). In contrast Pt and Pd (the PPGEs) and Au are incompatible during melting of the mantle in the absence of sulphides (Mungall & Brenan, 2014), resulting in fractionation of the PGEs during mantle melting after the sulphides have been melted out. The constraints obtained from PGE and Au on the composition and melting dynamics of the mantle are therefore complementary to those attained from the lithophile elements.

There are reports of PGE and Au compositions for CAMP rocks (Gottfried & Froelich, 1988; Gottfried *et al*., 1991; Kutina *et al*., 1992; Greenough & Fryer, 1995), but this contribution is

the first to use the PGE and Au geochemistry to examine mantle melting dynamics in detail. We carried out forward modelling of the PGE and Au compositions of mantle melts simulating the mantle sources proposed for CAMP, following, e.g., Rehkämper *et al*. (1999) and Mungall & Brenan (2014). Moreover, the PGE modelling is combined with modelling of the lithophile rare earth elements (REE) and high-field strength elements (HFSE), following Momme *et al*. (2006). To this end we use the forward model REEBOX PRO, which simulates adiabatic decompression melting using the most recent thermodynamic and experimental constraints for mantle melting reactions and mineral-melt partition coefficients (Brown & Lesher, 2016). The goal is to combine the inferences from PGE, Au, REE and HFSE modelling to guide the interpretation of the mantle dynamics during the petrogenesis of the Morrocan CAMP flood basalts. We constrain the composition, lithology, temperature, degree of melting, depth of mantle melting and upwelling dynamics, and discuss the geodynamics and origin of CAMP flood basalt volcanism. Finally, we discuss the prospectivity of CAMP for PGE deposits.

BACKGROUND STRATIGRAPHY, COMPOSITION AND AGE OF CAMP

The magmatic rocks of CAMP are typically evolved basalts to basaltic andesites. They form sills, dykes, and lava flow piles up to 400 m thick. Most CAMP rocks can be described as low-Ti (<2.4 wt % TiO_2) basalts and have been subdivided into six main groups on geochemical grounds (Marzoli *et al*. 2018) as described in the following. The oldest low-Ti group is represented by the lowermost lava unit (Lower unit) from Morocco, together with dykes and sills of similar composition from NW Africa they are also referred to as the Tiourjdal geochemical group with a geographical extent as shown in Fig. 1 (Marzoli *et al*., 2018; in revision). In Morocco, the Lower lava unit is successively overlain by the Intermediate and Upper lava units. Sills and dykes, of similar composition to these two lava units, have been recognised across the entire CAMP area (Fig. 1). Together they make up the low-Ti Prevalent geochemical group (Marzoli *et al*., 2018). Lastly, the Recurrent unit represents the stratigraphically youngest volcanic flows in CAMP. In Africa, the Recurrent unit is represented by a single, thick lava flow restricted to the High Atlas Mountains of Morocco, and dykes in south Morocco and Algeria. In the Newark Basin, NE America, flows and dykes of similar composition occur. These magmatic rocks are also low-Ti and together make up the Recurrent geochemical group outcropping as shown in Fig. 1 (Marzoli *et al*., 2018; in revision). In addition, there are dyke swarms, and also sills and lavas in NE America that

have been identified as two separate low-Ti geochemical groups (Carolina and Holyoke, not shown in Fig. 1) (Callegaro *et al*., 2013; Marzoli *et al*., 2018). These two groups are geochemically close to the Prevalent group, and do not crop out in Morocco. Finally, CAMP also includes a High-Ti geochemical group (1.6-4.1 wt % TiO_2) composed of dykes, sills, lavas and the Freetown Layered Intrusion outcropping in NE South America and southern NW Africa (not shown in Fig. 1) (Deckart *et al*., 2005; Merle *et al*., 2011; Callegaro *et al*., 2017). In Morocco, the most complete lava succession; including Lower, Intermediate, Upper and Recurrent units, is exposed in the Central High Atlas Mountains, and is the focus of the present study. The studied rocks are thus representative of most of the low-Ti magma types known in CAMP.

The Lower, Intermediate and Upper lava units of Morocco make up a volcanic succession with only a few and thin interbedded sediments (Fig. 2) (Marzoli *et al*., 2004; Knight *et al*., 2004; Panfili *et al*., 2019). In contrast, the Recurrent lava unit is separated from the Upper lava unit by 30-50 m of sediments (Marzoli *et al*., 2004; Knight *et al*., 2004; Panfili *et al*., 2019). Identical spore-pollen assemblages in the sediments immediately below and above the package of Lower to Upper lava units suggest that this volcanic succession erupted during the end-Triassic mass extinction interval (Panfili *et al*., 2019). This is confirmed by recent high-precision U-Pb zircon chronology (n=19), with ages ranging from 201.635 ± 0.029 Ma to 201.274 ± 0.032 Ma for the package from Lower to Upper lava units and intrusive equivalents from all four continents (Blackburn *et al*., 2013; Davies *et al*., 2017; Heimdal *et al*., 2018; Marzoli *et al*., in revision). Altogether, the palynology and U-Pb chronology indicate that the volcanic package comprising Lower to Upper lava units and intrusive equivalents was emplaced in less than 200.000 years (Blackburn *et al*., 2013; *Davies et al*., 2017; Panfili *et al*., 2019; Marzoli *et al*., in revision). In marine sediments, the coincidence of tracers of CAMP volcanism (ash layers, mercury anomalies) and tracers of ecosystem and paleoclimate perturbations (carbon isotope excursions and fossils) has prompted the interpretation that the end-Triassic mass extinction was caused by CAMP (Blackburn *et al*., 2013; Dal Corso *et al*., 2014; Thibodeau *et al*., 2016; Lindström *et al*., 2017; Yager *et al*., 2017; Percival *et al*., 2017; Davies *et al*., 2017; Heimdal *et al*., 2018; Panfili *et al*., 2019). Finally, recent chronology shows the Recurrent group in Morocco (201.15 ± 0.70 Ma $^{40}Ar/^{39}Ar$ age; Marzoli *et al*., in revision) and in NE America (200.916 ± 0.032 Ma U-Pb age; Blackburn *et al*., 2013) is slightly younger than the main volcanic package of Lower to Upper lava units, consistent with the intervening 30-50 m of sediment.

SAMPLES

We examined a total of 31 lava samples mainly from the classic section at Tiourjdal and Agouim in the Central High Atlas Mountains, and supplemented these with samples from the Argana Valley and Ait Ourir (Fig. 2). This selection represents the most complete volcanic package of CAMP from the Lower to the Recurrent lava units, and is thus representative of the main geochemical groups apart from the High-Ti group (Marzoli *et al*., 2018). In the Tiourjdal area the lavas dip gently to the south (12-15°), and make up the thickest and most complete lava succession known in Morocco (Fig. 2) (Marzoli *et al*., 2004, in revision; Knight *et al*., 2004). The details of field relations are summarised in Supplementary Data file 1 and a sample list is given in Supplementary Data file 2. At Tiourjdal we sampled all the major lava flows (n = 21) from the base near the river Driss to the uppermost flow below the overlying sediments; our GPS and altimeter measurements suggest the stratigraphic thickness of the volcanic package is c. 250m. The basal contact to the underlying sediments was not exposed due to high water stand, but is assumed to be located in the river bed (Dal Corso *et al*., 2014). Following Knight *et al*. (2004), Marzoli *et al*. (2004; in revision) and adding our observations, the Tiourjdal section (Fig. 2) can be divided into: (1) a c. 103 m thick Lower lava unit (n = 7) composed mainly of 0.1-0.5 m thick massive pahoehoe flow lobes separated by more rubbly and porous volcanic material, but also including a simple sheet flow (c. 9 m thick) in the upper portion; at least the lower package below the sheet flow may well represent one compound cooling unit (El Hachimi *et al*., 2011; Marzoli *et al*., 2018); (2) a c. 122 m thick Intermediate lava unit (n = 11) composed mainly of pahoehoe flow lobes similar to the Lower unit, but also including 2 sheet flows (9 and 13 m thick). A notable feature also described by Knight *et al*. (2004) is the presence of a 1 m thick limestone unit about half way up in the Intermediate unit that is overlain by a c. 10 m thick layer of pillow basalt; and (3) a c. 25 m thick Upper lava unit composed of three sheet flows (n = 3). This package of Lower, Intermediate and Upper unit volcanic rocks is overlain by a c. 50 m thick sedimentary succession, followed by a massive, columnar jointed lava flow that is c. 15 m thick and represents the Recurrent unit. The Recurrent unit was sampled (n = 2) in the exposures at Agouim a few km from Tiourjdal (Marzoli *et al*., 2004; Knight *et al*., 2004). The Recurrent unit is remarkable in the way that it makes up one single, thick lava flow, interbedded in the sedimentary series of the Central High Atlas. Geochemically similar flows and dykes have also been recognised in northeastern USA, and as dykes in the Anti Atlas and Algeria, and are shown as the Recurrent group in Fig. 1 (Marzoli *et al*., 2018). Lastly, our sample

set also includes samples (n = 7) of Lower and Intermediate lava units from the Argana Valley (mainly from the Tazantoute section also described by Deenen *et al*., 2011), and one sample of the Recurrent lava unit at Ait Ourir in the northern Central High Atlas Mountains (Fig. 1).

METHODS

The whole-rock compositions of the 31 sample were measured at Bureau Veritas Commodities Canada Ltd by X-ray fluorescence (major elements) and by inductively coupled plasma-mass spectrometry (trace elements) and reported in Table 1 (see Supplementary Data file 3 for details). Analyses of certified reference materials show that the relative deviation from the reference values is less than 3% for the major elements, less than 9% for the trace elements discussed in this paper apart from U (up to 10%), Cs (up to 10%), Ta (up to 12%) and Tm (up to 15%) (Supplementary Data file 4). Repeat analyses demonstrate reproducibility within 3% for the major elements (four samples), and within 7% (two samples) for trace elements, with the exception of Cs (up to 20%), Ta (25% in one sample) and Lu (22% in one sample) (Supplementary Data file 5).

The whole-rock concentrations of platinum group elements (PGE) and gold (Au) were analysed at Cardiff University for a subset of 12 samples, using nickel sulphide fire assay pre-concentration and tellurium co- precipitation, followed by inductively coupled plasma-mass spectrometry. Fifteen grams of sample were mixed with the reagents Na-carbonate, borax, sulphur, carbonyl-purified Ni, and silica. Subsequently, the solution was transferred into a fire-clay crucible and fired for 90 min at 1000 deg C (Huber *et al*., 2001). Afterwards, the buttons were spiked with 0.1 ml of a 2500 ppb In and Tl solution and dissolved with 3 ml concentrated HNO_3 and 4 ml concentrated HCl. The dissolved PGE and Au were then transferred to a 50ml flask that was supplemented up to the rim with 18.2 MΩ de-ionised water. Finally, the solution was analysed on a Thermo X Series 2 ICP-MS system. The certified reference materials WITS1, TDB1, and WPR1 were analysed together with the unknowns and, for most, fall within the standard error of the reference material, although this does not apply for Ir, Pd and Au for TDB1 (Supplementary Data file 6). The measured PGE and Au concentrations are at least 10 times larger than the minimum detection limit for the method (McDonald & Viljoen, 2006) (Supplementary Data file 7). Duplicate analyses of three samples generally deviate less than 13%, apart from Rh deviating 22% and 32% in two samples, respectively, and Os deviating 22% in one sample.

RESULTS

Lithophile elements

The chemical stratigraphy of the Tiourjdal section shows the main compositional features of the lava units in Morocco (Fig. 3) and corroborates previous studies (Bertrand *et al*., 1982; Marzoli *et al*, 2004; in revision; Youbi *et al*., 2003; Deenen *et al*., 2010). The SiO_2 contents of the Lower and Intermediate units (49.6 – 53.7 wt %) straddle the classification boundary between basalt and basaltic andesite at 52 wt % (Le Bas *et al*., 1986), with no systematic stratigraphic variation (Fig. 3). SiO_2 is generally lower in the Upper lava unit (49.9 - 50.5 wt %) and even lower in the Recurrent lava unit (47.8 - 48.7 wt %). Upper and Recurrent rocks are, therefore, all basaltic. All the studied samples classify as quartz tholeiites and for simplicity we will refer to all as tholeiitic basalts, or basalts. The basalts of the Tiourjdal section are all evolved, with MgO between 8.7 and 5.7 wt % and without a systematic stratigraphic trend (Fig. 3). A well-recognised feature of the CAMP basalts is the remarkably well-defined units in terms of distinct minor and trace element compositions that can be correlated across continents (Marzoli *et al*., 2004, 2018, in revision; Blackburn *et al*., 2013). This distinction between lava units is particularly well demonstrated in the Tiourjdal section (Fig. 3). Here the Lower unit is the most enriched in incompatible elements such as TiO_2 (1.3 - 1.7 wt %) and Nb (9-13 ppm), and is followed upsection by lower concentrations in the Intermediate unit (1.1 – 1.4 wt % TiO_2; 7-8 ppm Nb) and even lower concentrations in the Upper unit (1.0 – 1.1 wt % TiO_2; 4-5 ppm Nb). It can also be noted that flows with distinct Lower and Intermediate unit compositions interfinger at the transition between the two units (as seen by the overlap of blue and orange symbols in Fig. 3). The composition of the Recurrent unit is also distinct from the other units (see below). At Tiourjdal, the Recurrent lava unit is characterised by relatively high TiO_2 (1.6 – 1.8 wt %) compared to the underlying units, but with Nb (4-5 ppm) similar to the Upper unit lavas.

The distinct trace element compositions of the four lava units are also illustrated when the whole dataset is plotted against MgO (Fig. 4). Although Nb plots in distinct fields for each unit, it increases with decreasing MgO within the Lower lava unit, and there are also indications of similar correlations in the other units. The compatible element Cr correlates positively with MgO in the whole dataset and shows some overlap between the units; however, the Lower unit generally shows a higher Cr content for a given MgO relative to the overlying units.

The rare earth element (REE) patterns are enriched in the light-REE relative to the heavy-REE for all the Moroccan lavas and show diminishing enrichment of LREE relative to chondrite upsection, from the Lower, to the Intermediate and the Upper lava units (Fig. 5). The Recurrent unit, in contrast, displays an unusual pattern with flat and elevated middle- to heavy-REE (20-30 times chondrite), and only slight enrichment of the light-REE relative to the heavy REE.

The multi-element patterns summarise the compositional features of the Moroccan CAMP lavas (Fig. 6). All four lava units display increasing enrichment from right (least incompatible elements) to left (most incompatible elements), but with distinct negative anomalies for Ti, P and Nb-Ta, and positive anomalies for Pb and Cs. While the patterns of the Lower, Intermediate and Upper units are very similar in the middle part of the diagram (U to Gd), the Lower unit is distinctly more enriched than the Intermediate unit, which in turn is more enriched than the Upper unit. The Intermediate unit shows the largest anomalies of the four units. The pattern for the Recurrent unit is generally parallel to the other units in the middle part of the diagram but shows a large negative Sr anomaly. Sr also shows minor negative anomalies in the Lower and Intermediate units. At the right-hand side of the diagram it can be seen that the Lower, Intermediate and Upper lava units have a steeper slope (e.g. higher Dy/Yb_N) relative to the Recurrent unit, which shows a nearly horizontal pattern with Dy/Yb_N close to 1.0, but at higher concentrations. At the left-hand side of the diagram there are also marked differences. Although the alkali elements are relatively mobile during fluid-driven alteration processes, their patterns appear to be systematic: (1) positive Cs relative to Rb and K in all four units; (2) pronounced negative Rb and K anomalies in the Upper and Recurrent units, but not in the Lower and Intermediate units; and (3) low Ba/Th in the Upper and Recurrent units compared to the Lower and Intermediate units.

Platinum group elements and gold

The platinum group elements (PGE) and Au are plotted in a primitive mantle-normalised diagram together with Ni and Cu (Fig. 7), making this diagram useful to evaluate elemental control by sulphides and/or chromite, either occurring as residual phases in the mantle or precipitating from the magma in the crust (Barnes *et al*., 1988). Control by sulphides will result in a bowl-shaped pattern with depletion in PGE and Au relative to Ni and Cu. The effect of chromite fractionation is depletion of Os and Ir, and in particular Ru relative to Pt, Pd, Au, Ni and Cu (Arguin *et al*., 2016). Moreover, Os, Ir and Ru, that are often referred to as IPGE (Ir-like PGE), are compatible in the silicates of the mantle (mainly olivine) and alloys or platinum group minerals associated with

chromite and/or olivine (Mungall & Brenan, 2014; Barnes *et al*., 2015; Arguin *et al*., 2016). In contrast, Pt and Pd (the PPGE) are incompatible during melting of the mantle in the absence of sulphide, while Rh is somewhere between the IPGE and PPGE, and Au generally behaves similar to PPGE during mantle melting.

In the dataset for the Moroccan lavas the concentrations of Pd and Pt range from 2 to 11 ppb and Au from 0.3 to 4.1 ppb, whereas all the IPGE are below 0.4 ppb (Table 1). No systematic stratigraphic variations are observed, either within unit, or overall, as illustrated for Pd in the Tiourjdal section (Fig. 3e). The mantle-normalised patterns in Fig. 7 are broadly similar for all lava units showing pronounced enrichment of PPGE and Au (c. 1-4 times primitive mantle) over IPGE (0.02 to 0.2 times primitive mantle), and distinct negative Ru anomalies. In the Moroccan lavas Ni is slightly more depleted than the IPGE, whereas Cu is slightly enriched relative to the PPGE and Au at 1-8 times primitive mantle (Fig. 7). The Recurrent unit shows the steepest trend with relatively low IPGE and Ni, relatively high PPGE, and the highest concentrations in the dataset for Au and Cu. Pd and Pt generally correlate positively (Fig. 8), and the Lower lava unit has higher Pt/Pd (1.1 – 1.7) than the Intermediate and Upper units (0.6 – 1.1), but similar to the Recurrent unit (1.2). One sample from the Lower lava unit (15M-16) is somewhat anomalous in the way it is relatively depleted in Pd and Au, but within the range of the other lavas for the remaining elements (Figs 7, 8).

MANTLE MELTING MODELS

In this section, we will first interpret the constraints provided by published Os isotope data, then the elemental data for the Moroccan lavas presented above, and follow this with the development and results of new mantle melting models. The goal is to examine the mantle melting dynamics resulting in CAMP magmatism by combining constraints from PGE, REE and HFSE elements.

Constraints from Os isotopes

Recently published Os isotope data provide key constraints on the CAMP mantle source. In Fig. 9a, the Os isotope compositions for low-Ti CAMP basalts show clear peaks at initial $^{187}Os/^{188}Os$ values of 0.130 both for the entire published dataset (n = 65 including Morocco) and for Morocco alone (n = 12) (Merle *et al*., 2011, 2014; Callegaro *et al*., 2013, 2014a; Marzoli *et al*., in revision). This confirms the inference that the Moroccan low-Ti basalts are representative of the entire province. Moreover, the peak value of 0.130 is indeed very similar to values expected for convecting,

asthenospheric mantle (Carlson, 2005), such as primitive upper mantle (PUM) that would have had a value of 0.1281 at 201 Ma (Meisel *et al*., 2001) (Fig. 9b). In contrast, recent and extensive Sr-Nd-Pb isotope data sets (not shown) have demonstrated that the compositions of low-Ti CAMP magmas are strongly influenced by the crust (Callegaro *et al*., 2013, 2014a; Merle *et al*., 2014; Whalen *et al*., 2015; Marzoli *et al*., 2018; in revision). All of these authors have argued that this dichotomy is best explained if the mantle beneath the Pangaean supercontinent was contaminated with continental crust.

As outlined by Whalen *et al*. (2015) and Shellnutt *et al*. (2018), this can be explained by continental sediments transported into the mantle by subducting slabs associated with the accretion of the Pangaea supercontinent. These authors present three key arguments in support of this inference. First, the amount of crustal contamination required to explain the Sr-Nd-Pb isotopes would be 20% crust (assuming a MORB-like mantle) and it is argued that the heat required to produce such extensive assimilation is unrealistically high. Second, the mantle-like Os isotope compositions do not allow for assimilation of more than 8% crust, even assuming a parental magma with $^{187}Os/^{188}Os$ as low as 0.120 (Marzoli *et al*., in revision). Third, the high Os concentrations of the mantle buffers the Os isotope compositions, even if mixed with significant amounts of crustal components.

The second and third arguments hinge on the composition of the crust that, in turn, is mainly controlled by the age, given the enormous differences in the parent/daughter ratio, Re/Os, between crust (ca. 8 in average upper crust, Saal *et al*., 1998) and mantle (ca. 0.08, McDonough & Sun, 1995). The crustal ages and geological histories of the host rocks to CAMP are obviously variable, given the large extent of the province across four continents (Fig. 1). However, in Morocco and NW Africa the upper crust was originally Archean and has been modified in orogenic cycles denoted as Eburnean (ca. 2 Ga), Pan-African (ca. 0.6 Ga), and Hercynian (ca. 0.3 Ga) events (Marzoli *et al*., 2017, and references therein). In N and S America the main orogenic cycles are Grenvillian (ca. 1.2 - 1.0 Ga), Brasiliano (ca. 0.6 Ga; in S America only), and multiple Paleozoic events denoted Caledonian and Appalachian (0.5 - 0.3 Ga; in N America only) (Gower & Krogh, 2002; Hatcher, 2010; Hibbard *et al*., 2010). To illustrate the effect of adding crust to the mantle in such orogenic events we have calculated the $^{187}Os/^{188}Os$ composition for potential crust at the time of CAMP (0.2 Ga). As an example, juvenile crust formed at 2 Ga with Re and Os compositions similar to average upper crust (Saal *et al*., 1998) would have reached $^{187}Os/^{188}Os$ compositions of 1.22 at 0.6 Ga and 1.54 at 0.2 Ga., see Fig. 9 caption. If this crust was added to the mantle at 0.6 Ga in a mixture

composed of 8% old continental crust and 92% PM, it would result in an $^{187}Os/^{188}Os$ value of 0.1293 at 201 Ma (Fig. 9b). This value is similar to the peak in the observed $^{187}Os/^{188}Os$ compositions for the CAMP low-Ti basalts. Using other reasonable assumptions for compositions and age of crust and mantle, or other mixing proportions of crust and mantle, would not change this conclusion.

The second argument against crustal contamination is also illustrated in Fig. 9. If the crust is old (2 Ga), modelling of coupled assimilation and fractional crystallisation (AFC; assumptions listed in Fig. 9 caption and Supplementary Data file 10) shows that $^{187}Os/^{188}Os$ of mantle-derived magma contaminated with 5% and 10% crust will be shifted to 0.1450 and 0.1750, respectively, and higher than the observed values for CAMP rocks (Fig. 9c). If the crust is younger, however, the effect of crustal assimilation is smaller and $^{187}Os/^{188}Os$ reaches values of 0.1312, 0.1363 and 0.1553 for 5%, 10% and 20% crustal assimilation, respectively (Fig. 9d). In principle, the Os isotope data allow for almost unlimited assimilation of juvenile (e.g. Hercynian) crust. However, in Morocco and NW Africa, the proportion of Hercynian crust is minor and not juvenile (Marzoli *et al*., 2017) and such crust is therefore highly unlikely to be dominant in any AFC processes. We have also not shown model results for assimilation of Grenvillian crust that is dominant in N America, but these models fall between those for 2 and 0.6 Ga crust shown in Figs. 9c and d. As argued by previous authors, the Os isotope composition of CAMP basalts allows for considerable crustal assimilation up to 10-12% crustal assimilation if the crust was restricted to the relatively young Pan-African rocks (Merle *et al*., 2011, 2014; Callegaro *et al*., 2013, 2014a; Marzoli *et al*., 2018, in revision). Even more assimilation would be allowed for the younger Caledonian-Appalachian crust in N America. However, the distribution of zircon ages in the sedimentary basins associated with CAMP volcanic rocks in Morocco and Canada show multiple peaks, always including peaks at ca. 0.6 Ga and ca. 2.0 Ga, often including a peak at ca. 1.0 Ga, and sometimes a peak at c. 0.3 Ga (Marzoli *et al*., 2017). This shows that CAMP was emplaced into a patchwork of crustal ages that would have had highly variable Os isotope compositions. Finally, Fig. 9e shows that initial $^{187}Os/^{188}Os$ is not correlated with the concentration of Th, which is sensitive to crustal contamination. We therefore conclude that the relatively tight peak in $^{187}Os/^{188}Os$ at 0.130 for low-Ti basalts across the entire CAMP province (Fig. 9a) is inconsistent with crustal assimilation playing a major role. However, the slight skewing of the peak to higher $^{187}Os/^{188}Os$ (broader to the right than to the left) may well be a result of minor crustal assimilation as argued by previous workers (Merle *et al*., 2011, 2014; Callegaro *et al*., 2013, 2014a; Marzoli *et al*., 2018, in revision). In contrast, the similarity between

the initial $^{187}Os/^{188}Os$ of the low-Ti basalts and mantle values (Figs 9a and b), and the indifference of the mantle Os budget to crustal input, strongly favours addition of crust to the mantle to explain the dichotomy between Sr-Nd-Pb and Os isotope compositions (Merle *et al*., 2011, 2014; Callegaro *et al*., 2013, 2014a; Marzoli *et al*., 2018, in revision).

Constraints from the lithophile elements

The incompatible lithophile element patterns for the Moroccan lavas are markedly different from the typical basalts of the ocean basins (N-MORB, E-MORB and OIB, Figs 5 and 6). Instead, they display many features akin to the composition of continental crust such as positive Pb and Cs anomalies, negative Nb-Ta, Ti and P anomalies, and a positive hump at Zr and Hf. This is typical for the low-Ti CAMP basalts (Prevalent geochemical group), which are similar across all four continents (Marzoli *et al*., 2018), and supports the inferences drawn from isotopes above. All four lava units described here from Morocco show these crust-like signatures, but there are several differences between the units that cannot easily be attributed to crustal contamination or crustal source lithologies, or to fractional crystallisation alone. For example, the difference in Nb concentrations in the four lava units is not easily explained by crustal processes (crystallisation, assimilation and/or magma mixing) (Fig. 4). Also, the variation in the ratio of MREE to HREE (e.g. Dy/Yb_N) is more likely controlled by residual garnet holding back the heaviest REE in the mantle, and hence relates to the depth, temperature and degree of mantle melting (Tegner *et al*., 1998). This can be illustrated in a diagram of Dy/Yb_N *vs* La/Sm_N (Fig. 10), where the latter ratio is a measure of the slope of the LREE patterns (Fig. 5). For the REE ratios shown in Fig. 10 the effect of fractional crystallisation is largely negligible, as demonstrated by a lack of correlation between these ratios and an index of fractionation such as MgO (Supplementary Data file 8). Likewise, a correlation with crustal assimilation is not indicated when these REE ratios are plotted against Th/Nb (Supplementary Data file 9), consistent with the inference from Os isotopes. If anything, the higher La/Sm_N in the Lower unit compared to the Intermediate unit (Fig. 10) is correlated with lower Th/Nb (Supplementary Data file 9); the opposite of the expectation for a control by crustal contamination or crust in the mantle source. La/Sm_N is also not anti-correlated with ΔNb (Supplementary Data file 9) as may be expected in the case of extensive crustal contamination in low-Ti continental flood basalt provinces (Luttinen, 2018). To illustrate the potentially modest effects of crustal assimilation, we have illustrated three examples of AFC on the REE ratios for the maximum amount (10%) of crustal assimilation allowed by the isotope compositions discussed

above (Callegaro *et al*., 2013, 2014a; Merle *et al*., 2014; Whalen *et al*., 2015; Marzoli *et al*., 2018; in revision). The three arrows denoted *i*, *ii* and *iii* in Fig. 10a show the calculated changes in a magma (average Upper unit magma) that has assimilated 10% of (*i*) Eburnean granitoid (average from Ennih & Liegeois, 2008), (*ii*) Pan-African granitoid (average from Toummite *et al*., 2013), and (*iii*) average continental crust of Albarède (2003). While the average continental crust represents bulk assimilation, the Eburnean granitoids are interpreted as crustal melts (Ennih & Liegeois, 2008) and the Pan-African granitoids as a mix of mantle and crustal melts (Toummite *et al*., 2013). We therefore consider them representative for the likely range of crustal components that may have been assimilated by the CAMP magmas. Clearly, crustal assimilation cannot explain the range of compositions in Fig. 10a. Below, we further show that crustal assimilation cannot explain the inter-unit variations in Th-Nb-Yb. We therefore interpret variations in Dy/Yb_N *vs* La/Sm_N (Fig. 10a) as mainly reflecting the mantle source composition, degree of melting and upwelling dynamics. The Lower, Intermediate and Upper lava units are fairly similar in Fig. 10a, and coincide with the compositional field for the prevalent low-Ti lavas identified across the entire CAMP. In detail, the Moroccan lavas, however, span a considerable range in Dy/Yb_N (1.15 – 1.45) and show the highest La/Sm_N in the Lower unit (2.0 - 2.6) and the lowest La/Sm_N (1.7 - 1.9) in the Upper unit, with the Intermediate unit in between. The Recurrent unit is very different, with much lower Dy/Yb_N (1.04 – 1.07) and also lower La/Sm_N (1.35 – 1.53), but compares to previously published data for this unit in Morocco and NE America.

The Th/Yb *vs* Nb/Yb plot also illustrates well the role of crustal components in CAMP magmas (Fig. 11a) (Whalen *et al*., 2015). This diagram combines the high-field strength elements Th and Nb with the HREE Yb and was introduced by Pearce (2008) to decipher crustal components (high Th/Nb) in mantle-derived basalts, and to constrain mantle dynamics. Pearce (2008) showed that basalts of volcanic arcs (crustal input to the shallow mantle via subduction) often plot in a parallel array displaced to higher Th/Yb for a given Nb/Yb relative to the oceanic mantle array (N-MORB, E-MORB, and OIB), whereas crustal contamination tends to produce an array that trends obliquely away from the oceanic mantle array. We have illustrated this oblique trend by adding three AFC curves in Fig. 11a showing magmas assimilating up to 30% crust. The Pan-African (Toummite *et al*., 2013) and Eburnean (Ennih & Liegeois, 2008) granitoids plot very similarly in this diagram and we have used the average composition of the Pan-African rocks in the AFC calculations. The AFC curves using N-MORB and E-MORB as starting magmas clearly trend obliquely not only to the mantle trend as argued by Pearce (2008), but also to the trend of the four

lava units in Morocco. This confirms that the compositional differences of the lava units in Morocco, and the general trend of low-Ti CAMP magmas, cannot be explained by variations in the amount of crustal assimilation. Moreover, these AFC models confirm the inference from isotopes discussed above that about 10% to 30% crustal assimilation by magmas derived from oceanic mantle types are required to explain the trace element compositions of low-Ti CAMP magmas. Finally, the AFC model starting with the average composition of the Upper lava unit also trends obliquely to the trend of the Moroccan lavas and, thus, does not provide a satisfactory explanation for the inter-unit variations. We therefore conclude that in this diagram, the Moroccan lavas define a tight trend similar to most other CAMP low-Ti basalts that is indeed displaced to higher Th/Yb and parallel to the oceanic mantle array, supporting the view of crustal input to the mantle via subduction.

Constraints from PGE, Au, Ni and Cu

The mantle-normalised patterns increasing from Ni over PGE, and Au to Cu (Fig. 7), show that the compositions of the Moroccan lavas are not controlled by sulphides. This demonstrates that sulphides must have been exhausted at least in parts of the mantle melting column (to release the PGE and Au to the melts), and that the lavas did not experience sulphide saturation and fractionation in a crustal magma plumbing system (Barnes *et al*., 1988). The negative Ru anomaly indicates a control by chromite (and platinum group minerals and alloys associated with chromite), most likely during crustal fractionation processes (Arguin *et al*., 2016). The Pt/Pd ratios of the Lower and Recurrent lava units are similar to the asthenospheric mantle (1.15, Barnes *et al*., 2015), whereas the Intermediate and Upper units have slightly lower Pt/Pd (Fig. 8). The Pt/Pd of the subcontinental lithospheric mantle (SCLM) is well constrained from the cratons where kimberlites and other alkaline magmas have brought xenoliths to the surface; the most recent data suggest the Pt/Pd of the SCLM is higher than both primitive mantle and the Moroccan lavas, and ranges from 1.95 to 2.44 (Barnes *et al*., 2015; Tappe *et al*., 2017; Maier *et al*., 2017) (Fig. 8).

Before we can interpret the inference from Pt/Pd on the mantle dynamics of the Moroccan lavas it is necessary to evaluate the effects of fractional crystallisation. For example, in the East Greenland flood basalt succession it was shown that Pd and Pt behaved opposite during fractional crystallisation; Pd increased as an incompatible element, whereas Pt declined as a compatible element, resulting in highly variable Pt/Pd ratios (1.3 – 0.1) (Momme *et al*., 2002). This was explained by fractionation of Pt into platinum group minerals associated with chromite and olivine,

due to lower solubility of Pt relative to Pd in basaltic melts (Rehkämper *et al*., 1999). Recently, Mungall & Brenan (2014) have shown that the solubility of Pt in basaltic magma correlates strongly and positively with both oxygen and sulphur fugacities. Momme *et al*. (2002, 2006) assumed the sulphur contents of the East Greenland basalts were relatively high (900 – 2000 ppm), but always below sulphide saturation. More recent investigations, in contrast, contend that the East Greenland magmas may have had considerably lower sulphur contents (Keays & Tegner, 2016), thus suggesting that Pt/Pd in the east Greenland flood basalts may have been fractionated due to low solubility of Pt (Mungall & Brenan, 2014). In contrast, CAMP magmas from across the province have been shown to have high sulphur contents (up to 1900 ppm), calculated from sulphur in clinopyroxene (Callegaro *et al*., 2014b). Thus, the CAMP magmas may have been so rich in sulphur, although the PGE and Au data show that they did not reach sulphide saturation, that fractionation of Pt from Pd was minimal. This view is corroborated by the positive correlation of Pd and Pt (Fig. 8). We therefore conclude that Pt/Pd of the Moroccan lavas was not fractionated by platinum group minerals or alloys. In Fig. 8 we have illustrated the effect of 30% silicate fractionation, the maximum range of fractionation required between the least and the most fractionated compositions of the Moroccan lavas, following modelling of Marzoli *et al*. (in revision). This shows that fractional crystallisation alone cannot explain the range in Pd and Pt in Fig. 8. Hence, the degree of mantle melting and/or source heterogeneity must play a role in explaining the range of compositions in Fig. 8. In summary, the Pt/Pd of the Moroccan lavas points to the convecting mantle, not the SCLM, as the dominant source of the PGE. However, the slight differences in Pt/Pd between the lava units, and in particular the higher Pt/Pd of Lower unit sample 15M-16 (Fig. 8), perhaps indicate some contributions from the SCLM.

Modelling background

In this section, we develop the model of melting dynamically upwelling mantle using the REEBOX PRO application of Brown & Lesher (2016). This forward model calculates the composition of the incompatible lithophile trace elements in mantle melts using the latest thermodynamic and experimental constraints on melting reactions and mineral-melt partition coefficients, and can simulate passive and active upwelling scenarios, melting of several potential mantle lithologies (dry and wet peridotite, harzburgite, and pyroxenite) and allows for exploring variable mantle potential temperatures (T_P). The platinum group elements and gold were modelled off-line using the REEBOX PRO output files and, hence, the results are directly correlative with the modelled

lithophile element compositions. This approach of combining inferences from almost completely independent geochemical systems, the highly siderophile and the lithophile elements, has proven to be a powerful way for constraining mantle melting dynamics of LIPs (Momme *et al*., 2006).

The REEBOX PRO model assumes incremental batch (i.e. near-fractional) melting of the upwelling mantle (Brown & Lesher, 2016). This is simulated in a step-wise fashion where the melting column is subdivided into a finite number of decompression steps between the solidus and the base of the lithosphere. Each small decompression step involves melting and removal of the instantaneous melt, and recalculation of the trace element composition of the residual mantle (e.g., Wood, 1979). The instantaneous melt composition is calculated using the equation for non-modal batch melting, and the composition of the residual mantle is calculated by mass balance. In the next decompression step the previous residual mantle parcel moves up to slightly lower pressure (simulating upwelling) and melts again, producing a slightly more depleted residual mantle and so forth. All instantaneous melts generated within the melting region are pooled together to form an aggregated melt composition (equation 12 in Brown & Lesher, 2016). The model simulates two end-member scenarios for the 2D shape of melting region. The first is upwelling in a simple column and this form of the melting region is perhaps most relevant for axial upwelling in mantle plumes (Day *et al*., 2013), or a narrow zone of mantle upwelling associated with the rupture of thick, continental lithosphere (Momme *et al*., 2006). The other shape is a triangular melting region where melting takes place in upwelling mantle parcels but stops when convection turns to horizontal; it is therefore often referred to as the corner-flow model initially developed to simulate melting dynamics at mid-ocean spreading ridges (Plank & Langmuir, 1992; Rehkämper *et al*., 1999). Similar flow patterns of upwelling asthenosphere and a triangular melting region are also shown in dynamic models of continental rifting and breakup (Nielsen & Hopper, 2004; Armitage *et al*., 2009). The composition of the aggregate melts is quite different between the two models (Rehkämper *et al*., 1999; Momme *et al*., 2006; Brown & Lesher, 2016); this is due to the higher proportion of the low-degree melts from the bottom of the triangular melting region compared to a columnar melting scenario. Melting begins at the solidus intersection and the maximum degree of melting (F_{max}) is obtained at the upper apex of the melting region. In the triangular melting region, the average degree of melting is about half of F_{max} and is given by equation 28 of Brown & Lesher (2016). Throughout this work, we refer to F_{max} as the measure of the degree of melting. One of the key factors for simulating the composition of melts produced during dynamic mantle upwelling is the transition from garnet to spinel stability. In REEBOX PRO, garnet is stable on the pyrolite

peridotite solidus above 2.7 GPa, whereas spinel is stable on the solidus below 3 GPa (Brown & Lesher, 2016), producing a 0.3 GPa transition where both phases exist.

The PGE, Au, Cu and Ni compositions of mantle melts are modelled following previous investigations (e.g. Keays, 1995; Rehkämper *et al*., 1999; Momme *et al*., 2006; Mungall & Brenan, 2014). One difference is that we have linked the model calculations to the REEBOX PRO application so that the mantle melting conditions are identical to the lithophile element models described above. This was achieved by using the REEBOX PRO output files for offline calculations in Excel, using the same melt fractions for each step. As first outlined by Keays (1995), the basis for this modelling are the extremely high partition coefficients for PGE and Au into mantle sulphides (of the order of 10^5 to 10^6; Mungall & Brenan, 2014); this means that the PGE and Au are held back in the mantle until the last sulphides are melted out. A further control is that the IPGE (Os, Ir and Ru) are compatible in the silicates of the mantle (mainly olivine), alloys and/or platinum group minerals associated with chromite and/or olivine (Mungall & Brenan, 2014; Barnes *et al*., 2015; Arguin *et al*., 2016). In contrast, Pt and Pd (the PPGE) are incompatible in mantle silicates, while Rh is somewhere between IPGE and PPGE, and Au generally behaves similar to PPGE during melting. The model for the PGEs and Au is set up to calculate a bulk D for each step based on the mass fractions of sulphide and silicate in the mantle, and sulphide-melt and silicate-melt partition coefficients. The mass fraction of sulphide is calculated assuming the sulphide contains 35 wt % S, i.e. the mass fraction of sulphide equals the concentration of S (ppm) in the source divided by 0.35 and times 10^{-6} (Mathez, 1976; Rehkämper *et al*., 1999). Therefore, the key controls on the behaviour of PGE and Au in the model melts are the sulphur (S) content of the mantle, the S-solubility of the melt, the degree of melting and the shape of the melting region.

Results of modelling: lithophile elements

The inference from the isotopic compositions of the dominant and widespread low-Ti CAMP basalts is that their source is dominated by depleted MORB mantle (DMM) mixed with up to c. 5% continental crust (CC) that was translated to the mantle via subduction zone processes (Merle *et al*., 2014; Callegaro *et al*., 2013, 2014a; Whalen *et al*., 2015; Marzoli *et al*., 2018). We therefore start by modelling the lithophile elements in such a scenario and use the trace element compositions of Salters & Stracke (2004) for DMM and of Albarède (2003) for average CC. In all the modelling presented below, we used REEBOX PRO default temperature-dependent parameterisations for lithophile trace element partitioning in a pyrolite anhydrous peridotite lithology (e.g. Walter, 1998).

Results of the modelling are first summarised in Dy/Yb_N *vs* La/Sm_N space (Fig. 10). Initially we assume a mantle potential temperature T_P of 1430°C, that is 100°C above ambient mantle (ΔT_P), which is similar to independent estimates for T_P of CAMP magmatism (Herzberg & Gazel, 2009; Hole, 2015; Callegaro *et al*., 2013). In this model, it is possible to partly match the compositions of the Lower, Intermediate and Upper lava units of Morocco by mixing 1-3% CC into DMM, and assuming a triangular melting region (Fig. 10b). However, the samples with Dy/Yb_N above 1.35 are not matched in these models. Melting DMM alone can produce Dy/Yb_N >1.35, but for unrealistically low F_{max} (<2%). We also note that the models with 1-3% CC mixed into DMM only fit the data for modest degrees of melting (F_{max} of 2-5%, Fig. 10b). Much better fits to the data for the Lower, Intermediate and Upper lava units can be obtained by mixing CC with a pyrolite lithology having a primitive mantle composition (PM, Sun & McDonough, 1989). Figure 10c shows that mixtures of PM with 0 to 8% CC roughly span the field of the Lower, Intermediate and Upper lava units for a mantle T_P of 1430°C and assuming a triangular melting region. For example, the simulation of melting a source composed of 96% PM and 4% CC overlaps with the Lower lava unit for c. 8-15% melting (F_{max}), with the Intermediate unit for 12-20% melting, and with the Upper lava unit for 16-22% melting (Fig. 10c). Melts of PM alone at 1430°C fit with the highest Dy/Yb_N samples for 6-8% melting. In the models assuming pyrolite PM composition and T_P of 1430°C, melting begins at a pressure of 3.4 GPa, or c. 110 km depth. Alternatively, a similar coverage of the data field for the Lower, Intermediate and Upper lava units can be obtained by varying T_P from 1380°C to 1530°C (i.e. ΔT_P of 50 to 200°C). For example, melting a mixture of 96% PM and 4% CC within this temperature range fits with the Lower lava unit for 9-17% melting, the Intermediate unit for 12-20% melting, and the Upper lava unit for 20-26% melting (Fig. 10d). At ambient mantle T_P (1330°C) melting of the above-mentioned mantle composition is restricted largely to the spinel stability field, resulting in Dy/Yb_N values that are close to one (not shown), and thus smaller than the values observed in the Lower, Intermediate and Upper lava units.

The REE patterns of the Recurrent lava unit are distinct relative to the other lava units in Morocco (Figs 5 and 10). The flat MREE to HREE with Dy/Yb_N slightly above 1, at first glance suggest shallow melting restricted to the spinel stability field. Indeed, model curves for melting DMM alone at T_P of 1330°C, and a triangular melting region, can produce the Dy/Yb_N and La/Sm_N of the Recurrent unit (not shown). However, F_{max} would have to be very modest at 2-4%. In contrast, melting of PM at this temperature produce Dy/Yb_N (1.11-1.13) that are higher than those of the Recurrent unit (Fig. 10c). There are two other ways to model the composition of the

Recurrent unit. The first is by melting DMM mixed with 1-3% CC at 1430°C in a triangular melting region; these model curves coincide with the Recurrent unit for 10-15% melting (Fig. 10b), and represent melting intercepting the solidus at 3.0 GPa. The second possibility is to assume melting in a columnar melting region as illustrated in Fig. 10e. For example, melting a mixture of 96% PM and 4% CC at 1430°C matches the Recurrent unit for high degrees of melting (21-24%). Likewise, melting a mixture of 98% DMM and 2% CC at 1430°C in a columnar melting region also matches the Recurrent unit, but for more modest degrees of melting (5-7%). Finally, we note that the model for a columnar melting region also fits the data for the Lower, Intermediate and Upper units for a mixture, e.g., of 96% PM and 4% CC at 1430°C for 6-10% melting (Fig. 10e). However, as we will see below, this model is not supported by the modelling of the PGEs.

In the Th/Yb *vs* Nb/Yb diagram, the data for the Moroccan lavas also require a minor proportion of continental crust in the source (Fig. 11). The model curves for pure DMM and PM coincide with the oceanic mantle array, as they should, whereas the model curves are shifted upwards to higher Th/Yb for a given Nb/Y when CC is added to the source (Fig.11b). Although the modelled compositions from sources composed of either a mixture of 96% PM and 4% CC, or a mixture of 98% DMM and 2% CC, only overlap with the lowest Th/Yb values of the CAMP basalts, they form trends that are parallel to the Moroccan lavas, corroborating the view that the continental crust component in the CAMP rocks indeed is integrated in the source. The offset between the model curves and the data may relate to the assumptions about the partition coefficients in the model. Assimilation of continental crust into melt derived from melting DMM or PM alone would not form such a trend (Pearce, 2008). This is illustrated by two mixing curves between N-MORB and E-MORB, respectively, and average continental crust (Albarède, 2003) that are oblique to the oceanic mantle array, and to the CAMP trend (Fig. 11a).

Results of modelling: PGE and Au

The PGE and Au compositions of mantle melts are largely independent of the silicate mineralogy, and mainly depend on the source concentrations of S, PGE and Au and on the melting dynamics. Continental crust contains little PGE (e.g. 0.5 ppb Pt; Rudnick & Gao, 2003) and Au (1.5 ppb; Rudnick & Gao, 2003); inclusion of a few percent crust in the mantle source will therefore not change the PGE and Au concentrations significantly. First, we examine the potential roles of two end-member mantle components: convecting asthenospheric mantle that we refer to as primitive mantle (PM) and sub-continental lithospheric mantle (SCLM). The assessment of the PGE

concentrations in these two mantle components is mainly based on the comprehensive compilation of Barnes *et al*. (2015) for mantle rocks and melts, summarised in Table 2. They argued that a subset of orogenic peridotite samples is the best representative of the convecting asthenospheric mantle, in other words near pristine, primitive mantle that has not been affected by significant melt extraction or metasomatic refertilisation. We have combined these values with the Ni, Au and Cu concentrations of Salters & Stracke (2004) in the preferred composition we refer to as PM (Table 2). The modelling results would not be significantly different for other recent estimates for the convecting mantle such as those of Becker *et al*. (2006) and Fischer-Gödde *et al*. (2011). The assumed composition for the SCLM was calculated as an average of mantle xenoliths from the cratons compiled by Barnes *et al*. (2015) (Table 2), and is similar to the recent findings for mantle xenoliths from the Kaapvaal and Karelian cratons (Maier *et al*., 2017). The choice of the S content of the mantle plays a significant role in the amount of melting required to melt out the sulphides and release the PGE. The range considered by most workers is from 119 ppm S for DMM (Salters & Stracke, 2004) to 250 ppm S for PM (McDonough & Sun, 1995). However, Momme *et al*. (2006) concluded that the mantle source of the East Greenland flood basalts may be as little as 100 ppm S. Mungall & Brenan (2014) used a conservative value of 185 ppm S in their modelling. We therefore explore the effects of 119 ppm *vs* 185 ppm S for PM, and use 119 ppm S for SCLM. The partition coefficients follow Mungall & Brenan (2014), Brenan *et al*. (2003, 2005) and Rehkämper *et al*. (1999) (Table 2). Finally, we assume that the mantle melt can dissolve 1200 ppm S. This number is consistent with typical S contents in low fO_2 continental LIP basalts including CAMP (e.g., Self *et al*., 2008; Callegaro *et al*., 2014b) and is in the middle of the range assumed previously for mantle melts (Mathez, 1997; Rehkämper *et al*., 1999; Momme *et al*., 2006; Mungall & Brenan, 2014). The assumed S-solubility mainly bears on the calculated F_{max}; higher solubility in the melt leads to a quicker depletion of S in the mantle source, resulting in a decrease in the degree of melting required to melt out the sulphides.

Figure 12 shows that PM has a relatively flat pattern from Os to Au relative to chondrite, whereas the SCLM is enriched in IPGE relative to PPGE. The model melts inherit this pattern for low-degree melting, but produce fractionated patterns enriched in PPGE over IPGE after the sulphides are melted out (illustrated by the curves for 15% and 20% melting, F_{max}). The high-degree melts of PM produce a hump-shaped pattern for the PPGE and Au that resembles the Moroccan lavas, whereas the melts of the SCLM show a negative slope from Pt to Pd that is generally not seen in the Moroccan lavas. This difference is also illustrated in Fig. 8 where model

melts of PM (Pt/Pd = 1.2) roughly coincide with most of the Moroccan lavas for 12-17% melting (assuming 119 ppm S in PM). In contrast, the melts of the SCLM (Pt/Pd = 2.0) generally fall outside the dataset for the Moroccan lavas and other CAMP rocks in Fig. 8 (Gottfried & Froelich, 1988; Gottfried *et al*., 1991; Greenough & Fryer, 1995). One exception in the Moroccan dataset is sample 15M-16 that compares to SCLM melts.

Results of modelling: Combining PGE and REE

We end the modelling section by combining inferences from REE and PGE elements. Due to the vast difference in partitioning of Cu and Pd into sulphide (1500 *vs* 400,000; Table 2), the Cu/Pd ratio drops abruptly in melts produced when the sulphides are exhausted in the mantle as shown in a plot of Cu/Pd *vs* La/Sm_N (Fig. 12). Figure 13a shows model curves for melting of a mantle composed of 96% PM and 4% CC at 1430°C. It can be seen that the model curves assuming a triangular melting regime fits reasonably well to the Intermediate lava unit if the source contains 119 ppm S and melts by 12-16%. In this plot, the two data points for the Upper lava unit can be reproduced by higher degrees of melting of c. 18-20% for a mantle with 185 or 119 ppm S, respectively, in a triangular melting region. This is consistent with the inference from Fig. 10 that the REE compositions of the Upper lava unit are best explained by higher degrees of melting relative to the Intermediate and Lower lava units. The model curves for melting in a columnar melting region fit the Recurrent unit well for c. 17% melting of a source with 185 ppm S. Figure 13b explores the effects of increasing the mantle T_P to 1530°C (i.e. ΔT_P of 200°C) for a mantle composed of 96% PM and 4% CC with 185 ppm S. The temperature has almost no effect on the melt curves produced in a columnar melting region (the model curves for 1430°C and 1530°C in Figs 13a and 13b, respectively, are nearly identical). For a triangular melting region increasing the temperature shifts the melt to slightly higher La/Sm_N because the sulphides are melted out slightly earlier (Fig. 13b), but not enough for temperature to explain the compositional differences in this plot. We therefore conclude from Fig. 13 that the Lower and Intermediate lava units are best explained by a triangular melting region. In contrast, the Recurrent unit fits best with the model melts of a columnar melting region, in particular for a source composed of PM, with 185 ppm S, and melting c. 17%. It is also worth noting that melting a source dominated by DMM (with or without a few % CC) in a columnar melting region cannot explain the Recurrent lava unit, or any of the underlying lava units (Fig. 13b).

DISCUSSION

The mantle sources

The new modelling suggests that the lithophile trace elements in the Moroccan basalts are best explained by a mantle source that contains up to 8% continental crust, but typically less. This is remarkably consistent with the inference from Sr-Nd-Pb-Os isotope data published recently for the widespread low-Ti basalts across the CAMP (Callegaro *et al*., 2013, 2014a; Merle *et al*., 2011, 2014; Whalen *et al*., 2015; Marzoli *et al*., 2018, in revision). A significant difference, however, is that our modelling shows that the Moroccan low-Ti basalts are best explained if the composition of the dominant mantle component is similar in terms of trace elements to the primitive mantle (PM), and not to the depleted MORB mantle (DMM) as suggested hitherto on the basis of isotopes. For the Lower, Intermediate and Upper lava units this interpretation is reached from the combined analysis of PGE and REE (Fig. 13). For the Recurrent lava unit, the REE and HFSE data can be modelled with either DMM or PM (Figs 10, 11), but again the combined analysis of PGE and REE (Fig. 13) is best explained by assuming a source that was dominated by the primitive mantle (with a few % crust). In a companion paper, Marzoli *et al*. (in revision) carefully re-evaluated new and existing isotope data from Moroccan CAMP tholeiites and concluded that a primitive mantle with Sr-Nd-Pb isotopes similar to prevalent mantle (e.g. PREMA of Zindler & Hart, 1986; White, 2015) may be an important component in the low-Ti Moroccan lavas. The prevalent mantle component is recognised in many ocean island basalts (OIB) (Zindler & Hart, 1986) and LIPs (Jackson & Carlson, 2011), but following White (2015) we refer to it as a broad region in Sr-Nd-Pb space that is enriched relative to DMM, and without connotations to its geodynamic origin. Likewise, Callegaro *et al*. (2013) found that the low-Ti CAMP basalts in southeastern North America could be explained either by a PREMA-type mantle or a more depleted mantle. Isotopes of Sr, Nd and Pb are not conclusive in discerning between these two different mantle sources, given their broadly similar signatures. Additionally, we note that not only LIP magmas, but also OIB magmas, often are moderately enriched in PGE compared to MORB (Ireland *et al*., 2009; Day, 2013); it is therefore plausible also from the PGE geochemistry point of view that a prevalent-type mantle was important in the source of the low-Ti CAMP basalts.

The role of the subcontinental lithospheric mantle (SCLM) as a source for CAMP magmatism is also debated. Some workers explain the depletion of Nb and Ta relative to REE (Fig. 6) or the enriched Sr-Nd-Pb isotope compositions as a signature of melting SCLM that was

modified either by arc processes (Pegram, 1990; Puffer, 2001; Dorais & Tubrett, 2008) or by mantle plume metasomatism (Cebria *et al*., 2003). Others argue that these observations are better explained by melting asthenospheric mantle that contains recycled continental sediments translated by subduction processes (Callegaro *et al*., 2013, 2014a; Merle *et al*., 2011, 2014; Whalen *et al*., 2015; Marzoli *et al*., 2018; in revision). The present data and modelling of PGE, Au and Cu confirm that the data for the Moroccan lavas are best explained by melting of the asthenospheric mantle, not the SCLM (Figs 8, 12). In this context, it is worth considering the intial Os isotope ratio ($^{187}Os/^{188}Os_i$) that is often used to distinguish asthenospheric mantle sources from the SCLM (Carlson, 2005). The initial $^{187}Os/^{188}Os_i$ of CAMP rocks partly overlaps with the primitive mantle (Fig. 9), but for the Intermediate and Upper lava units several samples (mainly in Morocco) have lower values similar to the SCLM (Callegaro *et al*., 2013, 2014a, 2017; Merle *et al*., 2011, 2014; Marzoli *et al*., in revision). Marzoli *et al*. (in revision) explained the low $^{187}Os/^{188}Os_i$ samples as possibly resulting from assimilation of sulphides in the cratonic SCLM, and argued based on mass-balance considerations that the lithophile isotope systems remained largely unchanged by this assimilation. Similarly, the low Pd/Os of SCLM (0.6, Table 2) relative to the high Pd/Os (c. 50) of the Moroccan lavas suggest that the Pd (and Pt) concentrations of the melts would not be swayed much by such a reaction with the SCLM. One sample of the Lower lava unit (15M-16), however, is distinctly depleted in Pd and Au relative to Pt (Figs. 3, 7), and has Pt/Pd ratios similar to melts of SCLM (Fig. 8). However, the lithophile elements of this sample are not distinctly different from the other samples of the Lower lava unit. It therefore remains unclear whether the PGEs and Au of sample15M-16 witness a contribution from the SCLM.

A remarkable feature of the Moroccan lavas is the distinct trace element patterns of the four lava units, e.g. the up-section decrease in the concentration of incompatible elements such as Ti and Nb from the Lower to the Upper lava unit (Figs 3-6). Verati *et al*. (2005) explained similar variations in dykes in Mali as a result of increasing degree of melting of a common mantle source. Our results support a similar interpretation to explain inter-unit differences (see below), but it is also clear that the large spread in Dy/Yb_N within each volcanic unit and the lack of intra-unit positive correlation of Dy/Yb_N and La/Sm_N cannot easily be explained by variable degrees of melting (Fig. 10). Neither can it be explained by variations in the efficiency of pooling of melts from the melting region, which should produce trends parallel to the melting curves in Fig. 10 (Tegner *et al*., 1998). Instead, the modelling in Fig. 10 suggests that the intra-unit variations may be a result of variations in the proportion of continental crust mixed into the mantle source, and/or due

to variations in mantle potential temperature. On the short timescale of the Moroccan CAMP volcanism (i.e., the Lower to Upper units appears to have formed as four volcanic cooling units; Knight *et al*., 2004; El Hachimi *et al*., 2011), significant variations in mantle T_P are unlikely. Hence, we explain the intra-lava unit compositional variations by small variations in the proportion of continental crust embedded in the mantle source. This interpretation is intuitively reasonable, as it would be surprising if the translation of crustal components via subduction zones could result in a completely homogenous distribution. It is already remarkable that a small fraction of continental crust appears to be present in the mantle sources across most of the CAMP province (discussed further below), although regional variations have been detected and linked to continental inheritance (Callegaro *et al*., 2013, 2017; Merle *et al*., 2014; Whalen *et al*., 2015; Shellnutt *et al*., 2018).

The modelling also indicates that the S content of the mantle varied between the different lava units. The Intermediate unit is well modelled for a mantle containing 119 ppm S. Inspection of Fig. 13a indicates that the source of the Lower unit may have contained even less sulphur (not modelled). In contrast, the Upper and Recurrent lava units appear to be best modelled by melting a source with higher S content (185 ppm in the models). Hence, our data and modelling indicate that the S-content of the sources may have increased with time, and this possibly relates to mantle upwelling and geodynamics as discussed below.

Mantle melting and the geodynamics of continental rifting

One outcome of the mantle melting modelling is that not only the S-content of the mantle but also the shape of the melting region, and the degree of melting may have changed with time. If we disregard the intra-unit variations discussed above, the changing melting dynamics can be illustrated (Fig. 14) based on the model output for REE for upwelling primitive mantle mixed with 4% continental crust at constant mantle T_P (1430°C). These values represent the middle model curve through the data set in Fig. 10c. This analysis indicates that F_{max} increased from the Lower unit (8-16%), over the Intermediate unit (12-20%) and Upper unit (16-22%) to the Recurrent unit (21-24%), and also indicates changes in the shape of the melting region from triangular to columnar with time, as discussed above. Moreover, Fig. 14 illustrates that the intersection of the solidus at the bottom of the melting region was at c. 3.4 GPa (c. 110 km) and the top of the melting region changed from c. 1.5 GPa (c. 50 km) to c. 1 GPa (c. 32 km) with time. Our results based on trace elements are thus within the range of, but less extreme than independent estimates for the depth of

melting (4.5 to 0.3 GPa) based on petrological modelling of the major element compositions of CAMP magmatism (Herzberg & Gazel, 2009; Hole, 2015). As discussed by Hole (2015), the implication of these results is that significant stretching and thinning of the continental lithosphere is required to allow such shallow decompression mantle melting. This interpretation finds further support in dynamic models demonstrating that continental rifts can be associated with upwelling and melting of asthenospheric mantle under pressure and temperature conditions similar to our model results (Nielsen & Hopper, 2004; Armitage *et al*., 2009). Moreover, in the dynamic rift models the melting region beneath continental rifts typically develops a triangular shape, also supporting our modelling results.

In Morocco, the CAMP lavas are invariably associated with Triassic-Jurassic sedimentary basins (Knight *et al*., 2004; Marzoli *et al*., in revision). In contrast, the known dyke intrusions are mainly observed outside the rift basins (Fig. 1). A reconstructed structural map of North Africa, North America and South Eurasia (northern part of CAMP) at c. 200 Ma shows a plethora of sedimentary rift basins associated with the dispersal of Pangaea (Fig. 15) (El Harfi *et al*., 2006). Similar to Morocco, the known CAMP lavas in Eurasia and North America are also associated with basins (Olsen *et al*., 2002; Callegaro *et al*., 2014a; Merle et al., 2014; Marzoli *et al*., 2018). Although this observation may be biased due to basin inversion, other tectonics and erosion obliterating potential CAMP lavas erupted outside rift basins, it supports the association of CAMP extrusive volcanism and local continental rifts. In Morocco, there are differences in the occurrences of the volcanic units between rift systems (Marzoli *et al*., in revision). The Recurrent lava unit, for example, has only been identified in the Central High Atlas basins (Knight *et al*., 2004; Marzoli *et al*., in revision). We therefore speculate that the unusual composition of the Recurrent unit, that is best explained by relatively high degrees of melting in a columnar melting region, represents a late, transient, and low-volume melting event that was restricted to the Central High Atlas rift system. Magmas of the Recurrent group are, however, also identified as intrusions to the south of the Central High Atlas, and as extrusives and intrusives in northeast America (Fig. 1) (Marzoli *et al*., 2018, in revision). For the occurences in northeast America we speculate that rift systems and melting conditions similar to the Central High Atlas rift system existed. The low pressure indicated for the top of the melting region associated with the Recurrent lava unit (1 GPa, or 32 km depth, Fig. 13) suggests it was related to extensive upwelling. This is possibly similar to the formation of low-Ti basalts (interbedded with high-Ti basalts) in east Greenland, and explained by shallow, columnar melting thought to result from the incipient continental rupture (Tegner *et al*., 1998;

Momme *et al*., 2006). In east Greenland, it was argued that two rift systems and two separate mantle melting regions resulted in the co-eruption of two magma types. In Morocco, the Recurrent lava unit is separated from the Upper lava unit by c. 50 m of sediments and therefore clearly postdates the other lava units (Fig. 3). A slightly younger age for the Recurrent lavas, compared to the Lower to Upper flows, is also evidenced by new isotopic ages (Marzoli *et al*., in revision). The change from a dominantly triangular melting column to a columnar melting region for the Recurrent unit can be explained by the development of refractory, residual mantle in the upper part of the previous melting region that restricted melting (Tegner *et al*., 1998) (Fig. 13). The modelling of the PGE, moreover, indicates that the S-content of the source for the Recurrent unit may have increased relative to the underlying units, consistent with upwelling and melting of slightly different mantle material at this stage, possibly more plume-like mantle (Marzoli *et al*., in revision).

The geodynamics resulting in the emplacement of the dyke complexes outside the preserved rift basins remain unclear. In Morocco, we note that the two main known CAMP dykes (at Foum Zguid and Jbilet, Fig. 1) strike NE-SW and NNE-SSW, respectively, and this is approximately parallel to one of the dominating directions of the rift basins (Fig. 14) (Marzoli *et al*. (in revision). The emplacement of these dykes therefore appears to follow extensional tectonics similar to the well-developed rift systems. One possibility is that the dyke magmas propagated laterally away from the rift systems. It has been shown that dyke complexes may be injected laterally for more than 2000 km, e.g. the Mackenzie dyke swarm (Ernst & Baragar, 1992; Ernst, 2014). In Morocco, Marzoli *et al*. (in revision), for example, suggested that the Jbilet dyke was associated with the volcanics of the Argana rift. Likewise, the magma types identified in the Foum Zguid dyke can be correlated with the lava units in Morocco, including the Recurrent unit (Marzoli *et al*., 2018, in revision), suggesting a common origin.

We therefore conclude that the origin of the CAMP basalts in Morocco is best explained by melting anomalously hot, asthenospheric mantle upwelling mainly beneath continental rift zones as illustrated in Fig. 14.

Mantle plume and/or heating by super-continent insulation?

The ultimate challenge related to understanding CAMP magmatism, as for other LIPs, is to ascertain whether the mantle melting dynamics are associated with deep mantle plumes (e.g. Torsvik *et al*., 2006), and/or with mantle warming beneath super-continents (e.g. Coltice *et al*., 2007). In summary, the constraints from this study are: (*1*) the dominant mantle component appears

to be the convecting, primitive mantle producing PGE-rich basaltic magmas; (*2*) the role of the subcontinental lithospheric mantle is restricted, but may have contributed to a minor portion of the Moroccan CAMP, as indicated by one of the analysed samples showing high Pt/Pd; (*3*) the mantle source contained variable amounts up to 8% continental crust; (*4*) the mantle potential temperature was c. 1430 °C, i.e. about c. 100 °C warmer than ambient mantle. The CAMP magmatism presents several of the attributes often ascribed to melting of a mantle plume, such as coeval onset over a very large area, large volumes and rapid emplacement (Morgan, 1983; Hill, 1991; Wilson, 1997; Oyarzun *et al*., 1997; Ruiz-Martinez *et al*., 2012). Moreover, the paleo-placement of CAMP and the future line of breakup in the central Atlantic roughly coincide with a plume generation zone at the core-mantle boundary projected vertically to the surface (Torsvik *et al*., 2006; Svensen *et al*., 2018). In contrast, the unusual magma compositions are inconsistent with melting of mantle plume material; the magma compositions are very different from the normal mantle array as illustrated in Fig. 11. This offset from the mantle array cannot be explained by crustal contamination as discussed above and therefore supports inferences from Os isotopes that continental sediments were associated with the mantle source (Fig. 9) (Callegaro *et al*., 2013, 2014a, 2017; Merle *et al*., 2011, 2014; Marzoli et al., 2018; in revision). As pointed out by Pearce (2008), mantle plumes that have been argued to contain recycled continental crust only deviate slightly from the mantle array in Fig. 11. We therefore argue that the crustal component in the CAMP magmas is unlikely to have been an integrated part of a deep mantle plume. Hence, the crustal sediments in the source are best explained as a result of subduction processes associated with the assembly of Pangaea (Callegaro *et al*., 2013, 2014a, 2017; Merle *et al*., 2011, 2014; Whalen *et al*., 2015; Marzoli *et al*., 2018). This points to melting of the local mantle associated with the accretion of the Pangaea supercontinent. The similarity of the low-Ti magmas across the entire CAMP area further suggests that the subduction-related sediments were well mixed into the convecting mantle and thus distributed beneath Pangaea. This can be explained by an increase in the length-scale of mantle convection beneath super-continents, resulting in elevated mantle potential temperature (Coltice *et al*., 2007). Although the mantle potential temperature that this study and others (Herzberg & Gazel, 2007; Callegaro *et al*., 2013; Hole *et al*., 2015) find for CAMP is close to the upper limit possible from internal warming of mantle insulated by continental lithosphere ($\Delta T_P \leq 100$°C; Coltice *et al*., 2007), we argue that convection and heating of the asthenospheric mantle beneath Pangaea provide the best explanation for the nature of the mantle sources of CAMP low-Ti basalts. This does not rule out some mantle plume action. In particular, the coeval onset and correlation of magmatism across

most the CAMP province (Blackburn *et al*., 2013; Davies *et al*., 2017; Marzoli et al., 2018) appears best explained by mantle melting controlled by the arrival of a deep mantle plume. We therefore surmise that the arrival of a mantle plume may have triggered extensive continental rifting and CAMP volcanism (McKenzie & White, 1989), although melting would primarily be from the local asthenospheric mantle contaminated with crustal sediments. It is possible that the basalts of the Recurrent unit may partially represent the plume component, as discussed above and by Marzoli et al. (in revision). Other areas or units of CAMP outside Morocco may also represent the plume component (Callegaro *et al*., 2013; Marzoli *et al*., 2018).

Prospectivity for PGE and Au deposits

Platinum group elements and gold are enriched in the Moroccan CAMP lavas similar to the flood basalts of other large igneous provinces (Momme *et al*., 2002; Lightfoot & Keays, 2005; Jowitt *et al*, 2013; Hughes et al., 2015). The Moroccan magmas did not experience sulphide saturation during fractionation and the magmas were therefore fertile. This suggests that the CAMP province, as such, could be prospective for Ni-Cu-PGE mineralisation. One would have to look for ultramafic and mafic sills and plutons that were emplaced into S-bearing sediments that could react with the magmas and trigger sulphide saturation. For example, the sills emplaced into evaporite of the Amazonas and Sollimoes basins of Brazil (Heimdal et al., 2018) may be prospective targets. Alternatively, identification of evolved and fractionated layered intrusions may also be a target for Skaergaard-type Pd-Au mineralisation produced by prolonged fractionation in a closed-system magma chamber (Andersen *et al*., 1998; Nielsen *et al*., 2015; Keays & Tegner, 2016). Moreover, in contrast to the Skaergaard intrusion and the North Atlantic large igneous province, where Pt is fractionated from Pd as discussed above, this is not the case in the CAMP magmas (Fig. 8); this province therefore also holds the potential of Pt mineralisation. Indeed, Gottfried & Froelich (1988) have reported elevated Pd + Pt (225 ppb combined) in evolved ferrodiorite of the Palisades sill. Moreover, Os sulphide (ehrlichmanite) and Pt-Fe alloys nuggets have been reported in the eluvial, lateritic surface of the Freetown Layered Complex in Sierra Leone (Hattori *et al*., 1991), a gabbroic layered intrusion that has recently been demonstrated to be part of the CAMP (Callegaro *et al*., 2017). Analysis of the Os isotopic signatures of these nuggets allowed Hattori *et al*. (1991) to infer a magmatic origin for them. We therefore conclude that the CAMP magmas are fertile and therefore highly prospective for PGE and Au deposits.

CONCLUSIONS

Platinum group elements and gold are enriched in the Moroccan CAMP lavas similar to the flood basalts of other large igneous provinces. The magmas did not experience sulphide saturation during fractionation and the magmas were therefore fertile and, as such, the CAMP province is prospective for mineralisation. The Pt/Pd ratio shows that the Moroccan lavas originated by melting asthenospheric mantle, not the subcontinental lithosphere mantle. Mantle melting modelling of the REE, the HFSE and the PGE suggests:

(1) that the mantle source for all the lavas is dominated by primitive mantle and invariably includes a small proportion of continental crust (<8%);
(2) the mantle potential temperature was moderately elevated (c. 1430°C) relative to ambient mantle;
(3) intra-lava unit compositional variations are likely a result of variable amounts of the crust in the mantle source (heterogeneous source) and fractional crystallization;
(4) inter-lava unit compositional differences mainly reflect changes in mantle melting dynamics and minor changes in the mantle source composition (Recurrent unit);
(5) mantle melting initially took place at depths between c. 110 km and c. 55 km and became shallower with time (c 110 km to c. 32 km depth);
(6) the melting region changed from triangular to columnar with time (Fig. 14).

We explain these results by melting of asthenospheric mantle that was mixed with continental sediments during the assembly of Pangaea, then heated and further mixed by convection while insulated under the Pangaea super-continent, and subsequently melted in multiple continental rift systems associated with the breakup of Pangaea. We consider it likely that the CAMP volcanism was triggered by the arrival of a mantle plume, although the plume mantle apparently was not contributing much directly (chemically) to the magmas in Morocco and many other areas of CAMP.

ACKNOWLEDGEMENTS

This research was funded by the Danish National Research Foundation Niels Bohr Professorship grant 26-123/8, and by a Geocenter Denmark grant. Lara O'Dwyer Brown assisted with drafting of figures. The University of Padova, Italy, and a sabbatical stipend from Aarhus University Research Foundation to Chr. Tegner provided space and time to write this publication. Constructive reviews

by Arto Luttinen, Jim Mungall and an anonymous reviewer are much appreciated and helped to improve the manuscript.

REFERENCES

Albarède, F. (2003). *Geochemistry. An Introduction*. Cambridge: Cambridge University Press.

Andersen, J. C. O., Andersen, J. C. Ø., Rasmussen, H., Nielsen, T. F. D. & Ronsbo, J. G. (1998). The Triple Group and the Platinova gold and palladium reefs in the Skaergaard Intrusion; stratigraphic and petrographic relations. *Economic Geology* **93**, 488–509.

Arguin, J.-P., Pagé, P., Barnes, S.-J., Yu, S.-Y. & Song, X.-Y. (2016). The Effect of Chromite Crystallization on the Distribution of Osmium, Iridium, Ruthenium and Rhodium in Picritic Magmas: an Example from the Emeishan Large Igneous Province, Southwestern China. *Journal of Petrology* **57**, 1019–1048.

Armitage, J. J., Henstock, T. J., Minshull, T. A. & Hopper, J. R. (2009). Lithospheric controls on melt production during continental breakup at slow rates of extension: Application to the North Atlantic. *Geochemistry Geophysics Geosystems* **10**.

Barnes, S. J., Mungall, J. E. & Maier, W. D. (2015). Platinum group elements in mantle melts and mantle samples. *Lithos* **232**, 395–417.

Barnes, S.-J., Boyd, R., Korneliussen, A., Nilsson, L. P., Often, M., Pedersen, R. B. & Robins, B. (1988). The Use of Mantle Normalization and Metal Ratios in Discriminating between the Effects of Partial Melting, Crystal Fractionation and Sulphide Segregation on Platinum-Group Elements, Gold, Nickel and Copper: Examples from Norway. In: *Geo-Platinum 87*. Dordrecht: Springer Netherlands, 113–143.

Bas, M. J. L., Maitre, R. W. L., Streckeisen, A. & Zanettin, B. (1986). A chemical classification of volcanic rocks based on the total alkali-silica diagram. *Journal of Petrology* **27**, 745–750.

Becker, H., Horan, M. F., Walker, R. J., Gao, S., Lorand, J. P. & Rudnick, R. L. (2006). Highly siderophile element composition of the Earth's primitive upper mantle: Constraints from new data on peridotite massifs and xenoliths. *Geochimica Et Cosmochimica Acta* **70**, 4528–4550.

Bertrand, H., Dostal, J. & Dupuy, C. (1982). Geochemistry of early mesozoic tholeiites from Morocco. *Earth and Planetary Science Letters* **58**, 225–239.

Blackburn, T. J., Olsen, P. E., Bowring, S. A., McLean, N. M., Kent, D. V., Puffer, J. H., McHone, G. N., Rasbury, E. T. & Et-Touhami, M. (2013). Zircon U-Pb Geochronology Links the End-Triassic Extinction with the Central Atlantic Magmatic Province. *Science* **340**, 941–945.

Brenan, J. M., McDonough, W. F. & Ash, R. (2005). An experimental study of the solubility and partitioning of iridium, osmium and gold between olivine and silicate melt. *Earth and Planetary Science Letters* **237**, 855–872.

Brenan, J. M., McDonough, W. F. & Dalpé, C. (2003). Experimental constraints on the partitioning of rhenium and some platinum-group elements between olivine and silicate melt. *Earth and Planetary Science Letters* **212**, 135–150.

Brown, E. L. & Lesher, C. E. (2016). REEBOX PRO: A forward model simulating melting of thermally and lithologically variable upwelling mantle. *Geochemistry Geophysics Geosystems* **17**, 3929–3968.

Callegaro, S. *et al.* (2014a). Enriched mantle source for the Central Atlantic magmatic province: New supporting evidence from southwestern Europe. *Lithos* **188**, 15–32.

Callegaro, S., Baker, D. R., De Min, A., Marzoli, A., Geraki, K., Bertrand, H., Viti, C. & Nestola, F. (2014b). Microanalyses link sulfur from large igneous provinces and Mesozoic mass extinctions. *Geology* **42**, 895-898.

Callegaro, S. *et al.* (2017). Geochemical Constraints Provided by the Freetown Layered Complex (Sierra Leone) on the Origin of High-Ti Tholeiitic CAMP Magmas. *Journal of Petrology* **58**, 1811–1840.

Callegaro, S., Marzoli, A., Bertrand, H., Chiaradia, M., Reisberg, L., Meyzen, C., Bellieni, G., Weems, R. E. & Merle, R. E. (2013). Upper and lower crust recycling in the source of CAMP basaltic dykes from southeastern North America. *Earth and Planetary Science Letters* **376**, 186–199.

Carlson, R. W. (2005). Application of the Pt–Re–Os isotopic systems to mantle geochemistry and geochronology. *Lithos* **82**, 249–272.

Cebria, J. M., López-Ruiz, J., Doblas, M., Martins, L. & Munhá, J. (2003). Geochemistry of the early Jurassic Messejana- Plasencia dyke (Portugal-Spain): Implications on the origin of the Central Atlantic magmatic province. *Journal of Petrology* **44**, 547–568.

Coltice, N., Phillips, B. R., Bertrand, H., Ricard, Y. & Rey, P. (2007). Global warming of the mantle at the origin of flood basalts over supercontinents. *Geology* **35**, 391–394.

Dal Corso, J. *et al.* (2014). The dawn of CAMP volcanism and its bearing on the end-Triassic carbon cycle disruption. *Journal of the Geological Society* **171**, 153–164.

Davies, J. H. F. L., Marzoli, A., Bertrand, H., Youbi, N., Ernesto, M. & Schaltegger, U. (2017). End-Triassic mass extinction started by intrusive CAMP activity. *Nature Communications* **8**, 15596–8.

Day, J. M. D., Pearson, D. G. & Hulbert, L. J. (2013). Highly siderophile element behaviour during flood basalt genesis and evidence for melts from intrusive chromitite formation in the Mackenzie large igneous province. *Lithos* **182-183**, 242–258.

de Boer, J., and Snider, F. G. (1979). Magnetic and chemical variations of Mesozoic diabase dikes from eastern North America; evidence for a hotspot in the Carolinas?, *Geological Society of America Bulletin* **90**, 185-198.

Deckart, K., Bertrand, H. & Liégeois, J-P. (2005). Geochemistry and Sr, Nd, Pb isotopic composition of the Central Atlantic magmatic Province (CAMP) in Guyana and Guinea. *Lithos* 82, 289–314.

Deenen, M. H. L., Langereis, C., Krijgsman, W., Hachimi, El, H. & Chellai, E. H. (2011). Palaeomagnetic results from Upper Triassic red-beds and CAMP lavas of the Argana Basin, Morocco. *Geological Society, London, Special Publications* **357**, 195–209.

DePaolo, D. J. (1981). Trace element and isotopic effects of combined wallrock assimilation and fractional crystallization. *Earth and Planetary Science Letters* **53**, 189-202.

Dorais, M. J. & Tubrett, M. (2008). Identification of a subduction zone component in the Higganum dike, Central Atlantic Magmatic Province: A LA-ICPMS study of clinopyroxene with implications for flood basalt petrogenesis. *Geochemistry Geophysics Geosystems* **9**, doi: 10.1029–2008GC002079.

Ennih, N. & Liégeois, J. P. (2008). The boundaries of the West African craton, with special reference to the basement of the Moroccan metacratonic Anti-Atlas belt. In: Ennih, N., Liégeois, J.P. (Eds.), The Boundaries of the West African Craton. *Geological Society, London, Special Publication* 297, 1–17.

Ernst, R.E., and Baragar, W.R.A., 1992. Evidence from magnetic fabric for the flow pattern of magma in the Mackenzie giant radiating dyke swarm. *Nature* **356**, 511-513.

Ernst, R.E., 2014. Large Igneous Provinces. Cambridge University Press, United Kingdom 653 p.

Fischer-Gödde, M., Becker, H. & Wombacher, F. (2011). Rhodium, gold and other highly siderophile elements in orogenic peridotites and peridotite xenoliths. *Chemical Geology* **280**, 365–383.

Gottfried, D. & Froelich, A. J. (1988). Variations of palladium and platinum contents and ratios in selected early Mesozoic tholeiitic rock associations in the eastern United States. *United States Geological Survey Bulletin* **1776**, 322–341.

Gottfried, D., Froelich, A. J. & Grossman, J. N. (1991). Geochemical data for Jurassic diabase associated with early Mesozoic basins in the Eastern United States. *United States Geological Survey Open-File Report*.

Gower, C.F., and Krogh , T.E., 2002. A U-Pb geochronological review of the Proterozoic history of the eastern Grenville Province. *Canadian Journal of Earth Sciences* **39**, 795-829.

Greenough, J. D. & Fryer, B. J. (1995). Behavior of the platinum-group elements during differentiation of the North Mountain basalt, Nova Scotia. *The Canadian Mineralogist* **33**, 153–163.

Hachimi, El, H. *et al.* (2011). Morphology, internal architecture and emplacement mechanisms of lava flows from the Central Atlantic Magmatic Province (CAMP) of Argana Basin (Morocco). *Geological Society, London, Special Publications* **357**, 167–193.

Harfi, El, A., Guiraud, M. & Lang, J. (2006). Deep-rooted "thick skinned" model for the High Atlas Mountains (Morocco). Implications for the structural inheritance of the southern Tethys passive margin. *Journal of Structural Geology* **28**, 1958–1976.

Hatatcher, R.D.Jr. (2010). The Appalachian orogen: A brief summary. *Geological Society of America Memoirs* **206**, 1-19.

Hattori, K. H., Cabri, L. J. & Hart, S. R. (1991). Osmium isotope ratios of PGM grains associated with the Freetown Layered Complex, Sierra Leone, and their origin. *Contributions to Mineralogy and Petrology*. Springer-Verlag **109**, 10–18.

Heimdal, T. H., Svensen, H. H., Ramezani, J., Iyer, K., Pereira, E., Rodrigues, R., Jones, M. T. & Callegaro, S. (2018). Large-scale sill emplacement in Brazil as a trigger for the end-Triassic crisis. *Scientific Reports* **8**, DOI:10.1038–s41598–017–18629–8.

Herzberg, C. & Gazel, E. (2009). Petrological evidence for secular cooling in mantle plumes. *Nature* **458**, 619–622.

Hibbbard, J.P., van Staal , C.R., and Rankin, D.W. (2010). Comparative analysis of the geological evolution of the northern and southern Appalachian orogen: Late Ordovician–Permian. *Geological Society of America Memoirs* **206**, 51-69.

Hill, R. I. (1991). Starting plumes and continental break-up. *Earth and Planetary Science Letters* **104**, 398–416.

Hole, M. J. (2015). The generation of continental flood basalts by decompression melting of internally heated mantle. *Geology* **43**, 311–314.

Huber, H., Koeberl, C. & McDonald, I. (2001). Geochemistry and petrology of Witwatersrand and Dwyka diamictites from South Africa: search for an extraterrestrial component. *Geochimica Et Cosmochimica Acta* **65**, 2007–2016.

Hughes, H. S. R., McDonald, I. & Kerr, A. C. (2015). Platinum-group element signatures in the North Atlantic Igneous Province: Implications for mantle controls on metal budgets during continental breakup. *Lithos* **233**, 89-110.

Ireland, T. J., Walker, R. J. & Garcia, M. O. (2009). Highly siderophile element and 187Os isotope systematics of Hawaiian picrites: Implications for parental melt composition and source heterogeneity. *Chemical Geology* **260**, 112–128.

Jackson, M. G. & Carlson, R. W. (2011). An ancient recipe for flood-basalt genesis. *Nature* **476**, 316–319.

Jowitt, S. M., Williamson, M.-C. & Ernst, R. E. (2013). Geochemistry of the 130 to 80 Ma Canadian High Arctic Large Igneous Province (HALIP) Event and Implications for Ni-Cu-PGE Prospectivity. *Economic Geology* **109**, 281-307.

Keays, R. R. (1995). The role of komatiitic and picritic magmatism and S-saturation in the formation of ore deposits. *Lithos* **34**, 1–18.

Keays, R. R. & Tegner, C. (2016). Magma Chamber Processes in the Formation of the Low-sulphide Magmatic Au–PGE Mineralization of the Platinova Reef in the Skaergaard Intrusion, East Greenland. *Journal of Petrology* **56**, 2319–2340.

Knight, K. B., Nomade, S., Renne, P. R., Marzoli, A., Bertrand, H. & Youbi, N. (2004). The Central Atlantic Magmatic Province at the Triassic–Jurassic boundary: paleomagnetic and 40Ar/39Ar evidence from Morocco for brief, episodic volcanism. *Earth and Planetary Science Letters* **228**, 143–160.

Kutina, J., Bennani, A., Fredriksson, K., Nelen, J., Golightly, D. W., Brown, F. W., Brown, Z. A., Rait, N. & Moore, R. (1992). The Gabbro-Dolerite Magmatism of the Foum Zguid Region: Relation to Deep Structure of Morocco and Possible Potential for Cobalt, Nickel and Platinum-Group Metals. In: *Basement Tectonics 7*. Dordrecht: Springer, Dordrecht, 175–193.

Lightfoot, P. C. & Keays, R. R. (2005). Siderophile and Chalcophile Metal Variations in Flood Basalts from the Siberian Trap, Noril'sk Region: Implications for the Origin of the Ni-Cu-PGE Sulfide Ores. *Economic Geolog* **100**, 439–462.

Lindström, S., Pedersen, G. K., van de Schootbrugge, B., Hansen, K. H., Kuhlmann, N., Thein, J., Johansson, L., Petersen, H. I., Alwmark, C., Dybkjær, K., Weibel, R., Erlström, M., Nielsen, L. H., Oschmann,W. & Tegner, C. (2015). Intense and widespread seismicity during the end-Triassic mass extinction due to emplacement of a large igneous province. *Geology* **43**, 387–390.

Lindström, S., Erlström, M., Piasecki, S., Nielsen, L. H. & Mathiesen, A. (2017). Palynology and terrestrial ecosystem change of the Middle Triassic to lowermost Jurassic succession of the eastern Danish Basin. *Review of Palaeobotany and Palynology* **244**, 65–95.

Luttinen, A. V. (2018). Bilateral geochemical asymmetry in the Karoo large igneous province. *Scientific Reports* **8:5223**, doi:10.1038/s41598-018-23661-3.

Maier, W. D., O'Brien, H., Peltonen, P. & Barnes, S.-J. (2017). Platinum-group element contents of Karelian kimberlites: Implications for the PGE budget of the sub-continental lithospheric mantle. *Geochimica Et Cosmochimica Acta* **216**, 358–371.

Martins, L., Madeira, J., Youbi, N., Munhá, J., Mata, J. & Kerrich, R. (2008). Rift-related magmatism of the Central Atlantic magmatic province in Algarve, Southern Portugal. *Lithos* **101**, 102–124.

Marzoli, A., Bertrand, H., Knight, K. B., Cirilli, S., Buratti, N., Vérati, C., Nomade, S., Renne, P. R., Youbi, N., Martini, R., Allenbach, K., Neuwerth, R., Rapaille, C., Zaninetti, L. & Bellieni, G. (2004). Synchrony of the Central Atlantic magmatic province and the Triassic-Jurassic boundary climatic and biotic crisis. *Geology* **32**, 973–976.

Marzoli, A., Jourdan, F., Puffer, J. H., Cuppone, T., Tanner, L. H., Weems, R. E., Bertrand, H., Cirilli, S., Bellieni, G. & De Min, A. (2011). Timing and duration of the Central Atlantic magmatic province in the Newark and Culpeper basins, eastern U.S.A. *Lithos* **122**, 175–188.

Marzoli, A., Davies, J. H. F. L., Youbi, N., Merle, R., Dal Corso, J., Dunkley, D. J., Fioretti, A. M., Bellieni, G., Medina, F., Wotzlaw, J. F., McHone, G., Font, E. & Bensalah, M. K. (2017). Proterozoic to Mesozoic evolution of North-West Africa and Peri-Gondwana microplates: Detrital zircon ages from Morocco and Canada. *Lithos* **278-281**, 229-239.

Marzoli, A., Callegaro, S., Dal Corso, J., Davies, J. H. F. L., Chiaradia, M., Youbi, N., Bertrand, H., Reisberg, L., Merle, R. & Jourdan, F. (2018). The Central Atlantic Magmatic Province: A Review. In: Tanner, L. H. (ed.) The Late Triassic World, Springer doi:*1*0.1007/978-3-319-68009-5, 91–125.

Marzoli, A., Bertrand, H., Youbi, N., Callegaro, S., Merle, R., Reisberg, L., Chiaradia, M., Brownlee, S., Jourdan, F., Zanetti, A., Davies, J., Cuppone, T., Mahmoudi, A., Medina, F., Renne, P. R., Bellieni, G., Crivellari, S., El Hachimi, H., Bensalah, M. K., Meyzen, C. M., Tegner, C. (in revision). The Central Atlantic magmatic province (CAMP) in Morocco. *Journal of Petrology (in revision)*.

Marzoli, A., Bertrand, H., Chiaradia, M., Fontgnie, D., Youbi, N. & Bellieni, G. (2006). The genesis of CAMP basalts (Morocco) from enriched lithosphere to late asthenosphere mantle sources. Goldschmidt Conference abstract, doi:10.1016/j.gca.2006.06.799. Geochimica Et Cosmochimica Acta **A396**.

Mathez, E. A. (1976). Sulfur solubility and magmatic sulfides in submarine basalt glass. *Journal of Geophysical Research: Solid Earth* **81**, 4269–4276.

May, P. R. (1971), Pattern of Triassic-Jurassic Diabase Dikes around the North Atlantic in the Context of Predrift Position of the Continents, *Geological Society of America Bulletin* **82**, 1285-1292.

McDonald, I. & Viljoen, K. S. (2006). Platinum-group element geochemistry of mantle eclogites: a reconnaissance study of xenoliths from the Orapa kimberlite, Botswana. *Applied Earth Science* **115**, 81–93.

McDonough, W. F. & Sun, S. S. (1995). The composition of the Earth. *Chemical Geology* **120**, 223–253.

McHone, G. N. (2000). Non-plume magmatism and rifting during the opening of the central Atlantic Ocean. *Tectonophysics* **316**, 287–296.

Meisel, T., Walker, R. J., Irving, A. J. & Lorand, J.-P. (2001). Osmium isotopic compositions of mantle xenoliths: A global perspective. *Geochimica Et Cosmochimica Acta* **65**, 1311–1323.

Merle, R. E. *et al.* (2014). Sr, Nd, Pb and Os Isotope Systematics of CAMP Tholeiites from Eastern North America (ENA): Evidence of a Subduction-enriched Mantle Source. *Journal of Petrology* **55**, 133–180.

Merle, R. E., Marzoli, A., Bertrand, H., Reisberg, L., Vérati, C., Zimmermann, C., Chiaradia, M., Bellieni, G. & Ernesto, M. (2011). 40Ar/39Ar ages and Sr–Nd–Pb–Os geochemistry of CAMP tholeiites from Western Maranhão basin (NE Brazil). *Lithos* **122**, 137–151.

Momme, P., Tegner, C., Brooks, C. K. & Keays, R. R. (2002). The behaviour of platinum-group elements in basalts from the East Greenland rifted margin. *Contributions to Mineralogy and Petrology* **143**, 133–153.

Momme, P., Tegner, C., Brooks, C. K. & Keays, R. R. (2006). Two melting regimes during Paleogene flood basalt generation in East Greenland: combined REE and PGE modelling. *Contributions to Mineralogy and Petrology* **151**, 631–632.

Morgan, W. J. (1983). Hotspot tracks and the early rifting of the Atlantic. *Tectonophysic* **94**, 123–139.

Mungall, J. E. & Brenan, J. M. (2014). Partitioning of platinum-group elements and Au between sulfide liquid and basalt and the origins of mantle-crust fractionation of the chalcophile elements. *Geochimica Et Cosmochimica Acta* **125**, 265–289.

Nielsen, T. & Hopper, J. R. (2004). From rift to drift: Mantle melting during continental breakup. *Geochemistry Geophysics Geosystems* **5**, Q07003.

Nielsen, T. F. D., Andersen, J. C. Ø., Holness, M., Keiding, J. K., Rudashevsky, N. S., Rudashevsky, V. N., Salmonsen, L. P., Tegner, C. & Veksler, I. V. (2015). The Skaergaard PGE and Gold Deposit: the Result of in situ Fractionation, Sulphide Saturation, and Magma Chamber-scale Precious Metal Redistribution by Immiscible Fe-rich Melt. *Journal of Petrology* **56**, 1643–1676.

Olsen, P. E. *et al.* (2002). Ascent of Dinosaurs Linked to an Iridium Anomaly at the Triassic-Jurassic Boundary. *Science* **296**, 1305–1307.

Oyarzun, R., Doblas, M., López-Ruiz, J. & Cebria, J. M. (1997). Opening of the central Atlantic and asymmetric mantle upwelling phenomena: Implications for long-lived magmatism in western North Africa and Europe. *Geology* **25**, 727–730.

Panfili, G., Cirilli, S., Dal Corso, J., Bertrand, H., Medina F., Youbi, N. & Marzoli, A. (2019). New palynological constraints show rapid emplacement of the Central Atlantic magmatic province during the end-Triassic mass extinction interval. *Global and Planetary Change* 172, 60-68.

Pearce, J. A. (2008). Geochemical fingerprinting of oceanic basalts with applications to ophiolite classification and the search for Archean oceanic crust. *Lithos* **100**, 14–48.

Pegram, W. J. (1990). Development of continental lithospheric mantle as reflected in the chemistry of the Mesozoic Appalachian Tholeiites, U.S.A. *Earth and Planetary Science Letters* **97**, 316–331.

Percival, L. M. E., Ruhl, M., Hesselbo, S. P., Jenkyns, H. C., Mather, T. A., Whiteside, J. H. (2017). Mercury evidence for pulsed volcanism during the end-Triassic mass extinction. *Proceedings of the National Academy of Sciences* **114,** 7929–7934.

Plank, T. & Langmuir, C. H. (1992). Effects of the melting regime on the composition of the oceanic crust. *Journal of Geophysical Research* **97**, 19749–19770.

Puffer, J. H. (2001). Contrasting high field strength element contents of continental flood basalts from plume versus reactivated-arc sources. *Geology* **29**, 675–678.

Rehkämper, M., Halliday, A. N., Fitton, J. G., Lee, D. C., Wieneke, M. & Arndt, N. T. (1999). Ir, Ru, Pt, and Pd in basalts and komatiites: new constraints for the geochemical behavior of the platinum-group elements in the mantle. *Geochimica Et Cosmochimica Acta* **63**, 3915–3934.

Rudge, J. F. (2008). Finding peaks in geochemical distributions: A re-examination of the helium-continental crust correlation. *Earth and Planetary Science Letters* **274**, 179–188.

Rudnick, R. L. & Gao, S. (2003). Composition of the continental crust. *Treatise on geochemistry* **3**, 1–64.

Ruiz-Martínez, V. C., Torsvik, T. H., van Hinsbergen, D. J. J. & Gaina, C. (2012). Earth at 200 Ma: Global palaeogeography refined from CAMP palaeomagnetic data. *Earth and Planetary Science Letters* **331-332**, 67–79.

Saal, A. E., Rudnick, R. L., Ravizza, G. E. & Hart, S. R. (1998). Re–Os isotope evidence for the composition, formation and age of the lower continental crust. *Nature* **393**, 58–61.

Salters, V. J. M. & Stracke, A. (2004). Composition of the depleted mantle. *Geochemistry Geophysics Geosystems* **5**, doi:10.1029–2003GC000597.

Self, S., Blake, S., Sharma, K., Widdowson, M. & Sephton, S. (2008). Sulfur and Chlorine in Late Cretaceous Deccan Magmas and Eruptive Gas Release. *Science* **319**, 1654–1657.

Shellnutt, G., Dostal, J. & Yeh, M. W. (2018). Mantle source heterogeneity of the Early Jurassic basalt of eastern North America. *International Journal of Earth Sciences* **107**, 1033–1058.

Sleep, N. H. (1997). Lateral flow and ponding of starting plume material. *Journal of Geophysical Research*. **102**, 10001–10012.

Svensen, H. H., Torsvik, T. H., Callegaro, S., Augland, L., Heimdal, T. H., Jerram, D. A., Planke, S. & Pereira, E. (2018). Gondwana Large Igneous Provinces: plate reconstructions, volcanic basins and sill volumes. *Geological Society, London, Special Publications* **463**, 17–40.

Tappe, S., Brand, N. B., Stracke, A., van Acken, D., Liu, C.-Z., Strauss, H., Wu, F.-Y., Luguet, A. & Mitchell, R. H. (2017). Plates or plumes in the origin of kimberlites: U/Pb perovskite and Sr-Nd-Hf-Os-C-O isotope constraints from the Superior craton (Canada). *Chemical Geology* **455**, 57–83.

Tegner, C., Lesher, C. E., Larsen, L. M. & Watt, W. S. (1998). Evidence from the rare-earth-element record of mantle melting for cooling of the Tertiary Iceland plume. *Nature* **395**, 591–594.

Tegner, C., Wilson, J. R. & Robins, B. (2005). Crustal assimilation in basalt and jotunite: Constraints from layered intrusions. *Lithos* **83**, 299–316.

Thibodeau, A. M., Ritterbush, K., Yager, J. A., West, A. J., Ibarra, Y., Bottjer, D. J., Berelson, W. M., Bergquist, B. A. & Corsetti, F. A. (2016). Mercury anomalies and the timing of biotic recovery following the end-Triassic mass extinction. *Nature Communications* **7**, 11147–8.

Toummite, A., Liegeois, J. P., Gasquet, D., Bruguier, O., Beraaouz, E. H. & Ikenne, M. (2013). Field, geochemistry and Sr-Nd isotopes of the Pan-African granitoids from the Tifnoute Valley (Sirwa, Anti-Atlas, Morocco): a post-collisional event in a metacratonic setting. *Mineralogy and Petrology* 107, 739–763.

Torsvik, T. H., Smethurst, M., Burke, K. & Steinberger, B. (2006). Large igneous provinces generated from the margins of the large low-velocity provinces in the deep mantle. *Geophysical Journal International* **167**, 1447–1460.

Verati, C., Bertrand, H. & Féraud, G. (2005). The farthest record of the Central Atlantic Magmatic Province into West Africa craton: Precise Ar/Ar dating and geochemistry of Taoudenni basin intrusives (northern Mali). *Earth and Planetary Science Letters* **235**, 391–407.

Walter, M. J. (1998). Melting of garnet peridotite and the origin of komatiite and depleted lithosphere. *Journal of Petrology* **39**, 29–60.

Wessa, P. (2015). Kernel Density Estimation (v1.0.12) in Free Statistics Software (v1.2.1). *Office for Research Development and Education, URL* http://www.wessa.net/rwasp_density.wasp/

Whalen, L., Gazel, E., Vidito, C., Puffer, J. H., Bizimis, M., Henika, W. & Caddick, M. J. (2015). Supercontinental inheritance and its influence on supercontinental breakup: The Central Atlantic Magmatic Province and the breakup of Pangea. *Geochemistry Geophysics Geosystems* **16**, doi: 10.1002–2015GC005885.

White, R. & McKenzie, D. (1989). Magmatism at rift zones - The generation of volcanic continental margins and flood basalts. *Journal of Geophysical Research* **94**, 7685–7729.

White, W. M. (2015). Isotopes, DUPAL, LLSVPs, and Anekantavada. *Chemical Geology* **419**, 10–28.

Wilson, M. (1997). Thermal evolution of the Central Atlantic passive margins: continental break-up above a Mesozoic super-plume. *Journal of the Geological Society* **154**, 491–495.

Wood, D. A. (1979). Dynamic partial melting: its application to the petrogeneses of basalts erupted on Iceland, the Faroe Islands, the Isles of Skye (Scotland) and the Troodos Massif (Cyprus). *Geochimica Et Cosmochimica Acta* **43**, 1031–1046.

Yager, J. A., West, A. J., Corsetti, F. A., Berelson, W. M., Rollins, N. E., Rosas, S. & Bottjer, D. J. (2017). Duration of and decoupling between carbon isotope excursions during the end-Triassic mass extinction and Central Atlantic Magmatic Province emplacement. *Earth and Planetary Science Letters* **473**, 227–236.

Youbi, N., Martins, L., Munha, J. M., Ibouh, H., Madeira, J., Chayeb, E. & El-Boukhari, A. (2003). Triassic–Early Jurassic volcanism of Morocco and Portugal in the geodynamic framework of 1233 the opening of the Central Atlantic ocean. In: Hames, W. E., McHone, G. N., Renne, P. R. & Ruppel, P. R. (eds) *The Central Atlantic magmatic province Insights from fragments of Pangaea.*, 179–207.

Zindler, A. & Hart, S. (1986). Chemical geodynamics. *Annual Review of Earth and Planetary Sciences* **14**, 493–571.

FIGURE CAPTIONS

Figure 1: Schematic map of the Central Atlantic Magmatic Province (CAMP) showing the extent of flood basalts and intrusions in a c. 200 Ma reconstruction of the Pangaea Supercontinent. The restricted areal distribution of the Tiourjdal group (Lower lava unit in Morocco) and the Recurrent group (Recurrent lava unit in Morocco) are outlined. The dominant Prevalent low-Ti group (Intermediate and Upper lava units in Morocco) was emplaced over the entire CAMP area and is preserved on four continents today. Map and nomenclature after Marzoli *et al*. (2018).

Figure 2: (**a**) Google Earth™ map of central Morocco showing the main study areas (Tiourjdal and Argana) and sample locations. (**b**) The Tiourjdal volcanic succession studied here, showing lava unit boundaries following Knight *et al*. (2004).

Figure 3: Stratigraphic variations for selected, new major and trace element bulk-rock compositions for the CAMP basalts in the combined Tiourjdal and Agouim section, High Atlas, Morocco. The stratigraphic height is reported relative to the base of the volcanic succession.

Figure 4: Cr and Nb contents *vs* MgO of bulk-rock compositions for the four lava units of Morocco. The entire dataset of this study is shown, i.e., CAMP basalts from Tiourjdal and Agouim, High Atlas, and the Argana Basin.

Figure 5: Rare earth element (REE) patterns for the four lava units of Morocco, normalised to chondrite (Sun & McDonough, 1989). Also shown are typical patterns for normal and enriched mid-ocean ridge basalt (N- and E-MORB) and ocean island basalt (OIB) (Sun & McDonough, 1989).

Figure 6: Multi-element diagram for the four lava units of Morocco. For simplicity, the average compositions are shown. The elements are arranged with increasing compatibility in mantle rocks from left to right and normalised to primitive mantle (Sun & McDonough, 1989), except K that is placed next to the other alkali elements (Rb and Cs). Also, shown for comparison are typical patterns for continental crust (Albarède, 2003), normal and enriched mid-ocean ridge basalt (N- and E-MORB) and ocean island basalt (OIB) (Sun & McDonough, 1989).

Figure 7: Platinum group element, Au, Cu, and Ni patterns for the four lava units in Morocco normalised to primitive mantle (Os, Ir, Ru, Rh, Pt and Pd from Barnes *et al*., 2015; and Ni, Au and Cu from Salters & Stracke, 2004).

Figure 8: Pd *vs* Pt for the Moroccan lava units of this study. Also shown are: (i) a field for chilled margin compositions (i.e. liquid compositions) reported for other CAMP dykes, sills and lavas (n = 28; only rocks from northeastern USA have been analysed) from Gottfried & Froelich (1988), Gottfried *et al*., (1991), and Greenough & Fryer (1995); (ii) compositions of mantle lithologies (PM = convecting primitive mantle from Barnes *et al*. (2015), cratonic sub-continental lithospheric mantle (SCLM) from Barnes *et al*. (2015), Canadian SCLM from Tappe *et al*. (2016), and Karelian and Kaapvaal SCLM from Maier *et al*. (2017); (iii) modelled aggregate melts pooled from a triangular melting zone calculated for PM and for cratonic SCLM. Tick marks (1%) show the degree of mantle melting at the top of the melting region (F_{max}); (iv); the effect of 30% sulphide undersaturated fractional crystallisation is illustrated for a lava with 4 ppb Pt.

Figure 9: (**a**) Gaussian kernel density distribution of initial (201 Ma) osmium isotope compositions for low-Ti CAMP basalts from the entire province (including Morocco, n = 65; Merle *et al*., 2011, 2014; Callegaro *et al*., 2013, 2014a; Marzoli *et al*., in revision) and the Moroccan low-Ti basalts alone (n = 12; Marzoli et al., in revision). Both distributions peak at $^{187}Os/^{188}Os$ values close to 0.130. The kernel density estimations follow the method of Rudge (2008) and were calculated using the Free Statistics Software of Wessa (2015). (**b**) The Os isotope composition for Primitive Mantle (PM) back-calculated at 201 Ma (0.1281) using present-day primitive upper mantle (PUM) values ($^{187}Os/^{188}Os$ = 0.1296 and $^{187}Re/^{188}Os$ = 0.4350) as in Meisel *et al*. (2001). This panel also illustrates the shift in $^{187}Os/^{188}Os$ from mixing crustal material into mantle rocks. For example, adding 8% old (2 Ga) continental crust ($^{187}Os/^{188}Os$ = 1.22, 400 ppt Re and 50 ppt Os calculated following the average upper crustal values of Saal *et al*., 1998) to PM ($^{187}Os/^{188}Os$ = 0.1250, 280 ppt Re and 3400 ppt Os assuming mantle values of Meisel *et al*., 2001 and McDonough & Sun, 1995) at 0.6 Ga results in $^{187}Os/^{188}Os$ of 0.1293 at 201 Ma. This tiny shift in Os isotope values even from mixing with extremely radiogenic crust is due to the high Os concentrations of the mantle. **(c)** The shift in inital $^{187}Os/^{188}Os$ by crustal assimilation at 201 Ma calculated using the AFC equations of DePaolo (1981) and assuming the bulk partition coefficient for Os is 3 and the ***r***-value (ratio of the rate of mass assimilated to rate of mass crystallised) of 0.3 following Tegner *et al*. (2005). The

magma at 201 Ma is assumed to have mantle $^{187}Os/^{188}Os$ (0.1281) and 300 ppt Os (Marzoli *et al*., in revision, and equal to the highest concentration in our data set, Table 1). The crust is assumed to be old (2 Ga). We simulate assimilation of Eburnean crust with $^{187}Os/^{188}Os$ of 1.54 and 50 ppt Os assuming the average upper crustal values of Saal *et al*. (1998). In this case, the AFC model indicates that the $^{187}Os/^{188}Os$ of a magma that has assimilated 5% and 10% crust (i.e. instantaneous crust/magma ratio, Tegner *et al*., 2005) has shifted to 0.1450 and 0.1750, respectively. **(d)** Similar to (c), but assuming assimilation of younger crust (0.6 Ga) simulating reaction with Pan-African crust. In this case, the average upper crust can be assumed to have $^{187}Os/^{188}Os$ of 0.44 and 50 ppt Os at 201 Ma. The AFC model indicates that the $^{187}Os/^{188}Os$ of magma that has assimilated 5%, 10% and 20% crust has shifted to 0.1312, 0.1363 and 0.1553, respectively. The CAMP Os isotope data in (a) are from Merle *et al*. (2011, 2014), Callegaro *et al*. (2013, 2014a) and Marzoli *et al*. (in revision).

Figure 10: (**a**) Dy/Yb_N *vs* La/Sm_N for the Moroccan lava units of this study, together with a compositional field encompassing low-Ti basalts of the entire CAMP. Also shown is the effect of 10% crustal assimilation by coupled assimilation and fractional crystallisation (AFC) processes calculated as in Fig. 11. The starting magma composition is the average of the Upper unit low-Ti basalt of this study. Shown are the results for assimilation of (*i*) Eburnean granitoids (average from Ennih & Liegeois, 2008), (*ii*) Pan-African granitoids (average from Toummite *et al*., 2013), and (*iii*) average continental crust of Albarède (2003). (**b-d**) Results of forward modelling of aggregated liquids of mantle melting using REEBOX PRO (Brown & Lesher, 2016) and assuming a triangular melting region. The degree of melting at the top of the melting region (F_{max}) is given in %. (**b**) Model melts assuming the source is a mixture of depleted MORB mantle (DMM) and continental crust (CC); the proportion of CC is given in %. T_P is 1430°C. (**c)** Model melts assuming the source is a mixture of primitive mantle (PM) and continental crust (CC); the proportion of CC is given in %. T_P is 1430°C. **d)** Model melts assuming the source is a mixture of 96% PM and 4% CC (PM96) for variable mantle T_P (1380-1530°C). (**e)** Model melts assuming a columnar melting region and T_P of 1430°C for (i) a source that is a mixture of 96% PM and 4% CC (PM96) and (ii) a source that is a mixture of 98% DMM and 2% CC (DMM98). See text for further explanation. The compositional field for low-Ti CAMP basalts is based on data from: Alibert (1985); Dostal (1988); Papezik *et al*. (1988); Bertrand (1991); Heatherington & Müller (1999); Marzoli *et al*. (1999, 2004; in revision); De Min *et al*. (2003); Jourdan *et al*. (2003); Verati *et al*. (2005); Mahmoudi *et al*. (2007); Martins *et*

al. (2008); Merle *et al*. (2011, 2014); Callegaro *et al*. (2014); Bertrand *et al*. (2014); Whalen *et al*. (2015).

Figure 11: Th/Yb *vs* Nb/Yb. **(a)** The compositions of the Moroccan lava units of this study together with a compositional field encompassing low-Ti basalts of the entire CAMP. Also shown are the oceanic mantle array from Pearce (2008), the compositions of depleted mid-ocean ridge basalt (N-MORB), enriched mid-ocean ridge basalt (E-MORB), and ocean island basalt (OIB) from Sun & McDonough (1989), average continental crust from Albarède (2003), and the average composition of Pan-African granite in Morocco (Toummite *et al*., 2013). Three stippled curves show the results of modelled assimilation and fractional crystallisation (AFC) with tick marks showing % assimilated crust (average Pan-African granite, Toummite *et al*., 2013) from three starting magma compositions: N-MORM, E-MORB and average Upper Unit low-Ti basalt from this study. The AFC equations are from DePaolo (1981) and the calculations assume the bulk partition coefficients are 0.1 for all elements, and the ***r***-value (ratio of the rate of mass assimilated to rate of mass crystallised) is 0.3 (Tegner *et al*., 2005). The concentrations used in the AFC calculations are listed in Supplementary Data file 10. See Fig. 10 for a key to the Moroccan samples of this study, and for the sources of the compositional field for other CAMP low-Ti basalts. **(b)** The results of forward models of mantle melting using the REEBOX PRO simulation (Brown & Lesher, 2015) show melts produced in a triangular melting region at a T_P of 1430°C and by melting primitive mantle (PM) and depleted MORB mantle (DMM). Also shown are model melts from (i) a source composed of 96% PM mixed with 4% continental crust (CC) in a triangular melting regime (PM96_TMR), and (ii) a source composed of 98% DMM mixed with 2% CC and melting at 1430°C in a columnar melting region. Five % tick marks on all melting curves.

Figure 12: Chondrite-normalised Ni-PGE-Au-Cu patterns for: (i) the assumed compositions of primitive mantle (PM) and subcontinental lithospheric mantle (SCLM) (values in Table 2); (ii) modelled melts from partial melting at 0.01%, 5%, 10%, 15% and 20% (F_{max}) assuming 119 ppm S in the source; and (iii) the average composition of the Moroccan lavas of this study. Chondrite values from Sun & McDonough (1989).

Figure 13: Cu/Pd *vs* La/Sm_N for the Moroccan lava units of this study, also showing modelled melt compositions. **(a)** Modelled melts produced by melting a source composed of a mixture of 96%

primitive mantle and 4% continental crust (PM96) at a T_P of 1430°C. Results are shown for aggregated melts extracted from a triangular melting region (TMR) and from a columnar melting region (CMR), and for S-contents of 119 and 185 ppm in the source. **(b)** Here the modelled melts are again produced from the PM96 source as in (a) and containing 185 ppm S, but at T_P of 1430°C and 1530°C in triangular and columnar melting regions, respectively. Also shown are melts produced from DMM98 (a source composed of 98% DMM and 2% continental crust) in a columnar melting region. See text for further explanation.

Figure 14: Schematic illustration of possible mantle melting dynamics associated with the generation of CAMP basalts in Morocco in a continental rift system. The depth, the degree of melting (F_{max} = maximum degree of melting at the top apex of the melting region showing the maximum fitting the data in Fig. 9c), and the shape of the melting region are based on the REEBOX PRO model calculations assuming the mantle had a potential temperature of 1430°C and was composed of 96% primitive mantle and 4% continental crust. The paths of mantle upwelling are similar to those of dynamic melting models developing a triangular melting region during continental breakup (Nielsen & Hopper, 2004). The right-hand panel illustrates the potential position of residual and refractory mantle left over from previous melting, which possibly acted to restrict melting to a columnar region during the formation of the Recurrent lava unit. The figure also illustrates the model assumptions for the garnet to spinel transition between 3 and 2.7 GPa (in panel n. 3 from the left). The thicknesses of the sedimentary and volcanic basin are exaggerated.

Figure 15: Sketch map of the Triassic-Jurassic rift basins in the triple junction between North America, Eurasia and Africa. The strike of the basins changes from c. NE-SW in the Atlantic domain between North America and Africa to c. E-W in the Tethyan domain between Eurasia and Africa, and c. N-S between Eurasia and North America. Most of these basins are associated with CAMP volcanism (Knight *et al*., 2004; Marzoli *et al*., 2018; in revision), although CAMP volcanism dies out east of Morocco. Modified from El Harfi *et al*. (2006).

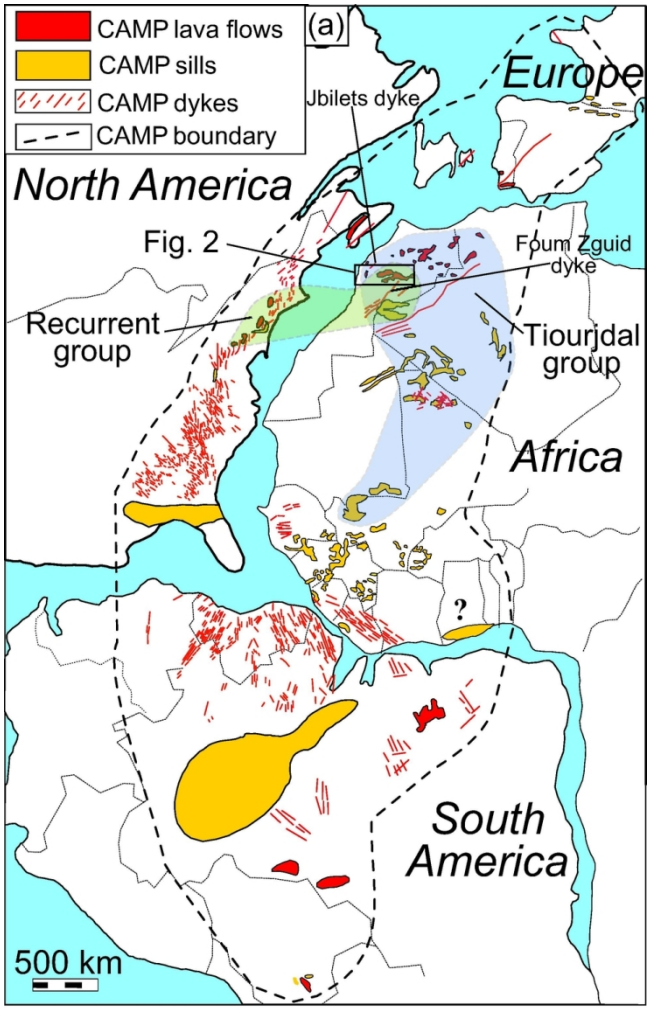

Figure 1 (Tegner et al., 2018)

Figure 1

83x155mm (300 x 300 DPI)

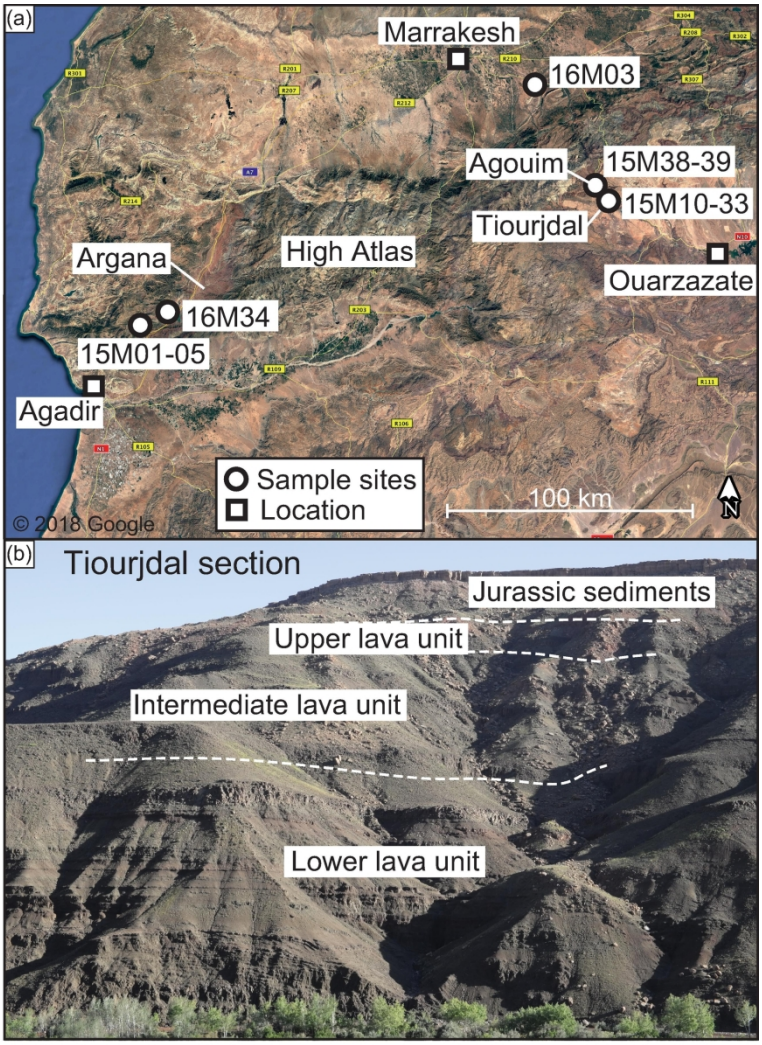

Figure 2 (Tegner et al., 2018)

Fig. 2

181x246mm (300 x 300 DPI)

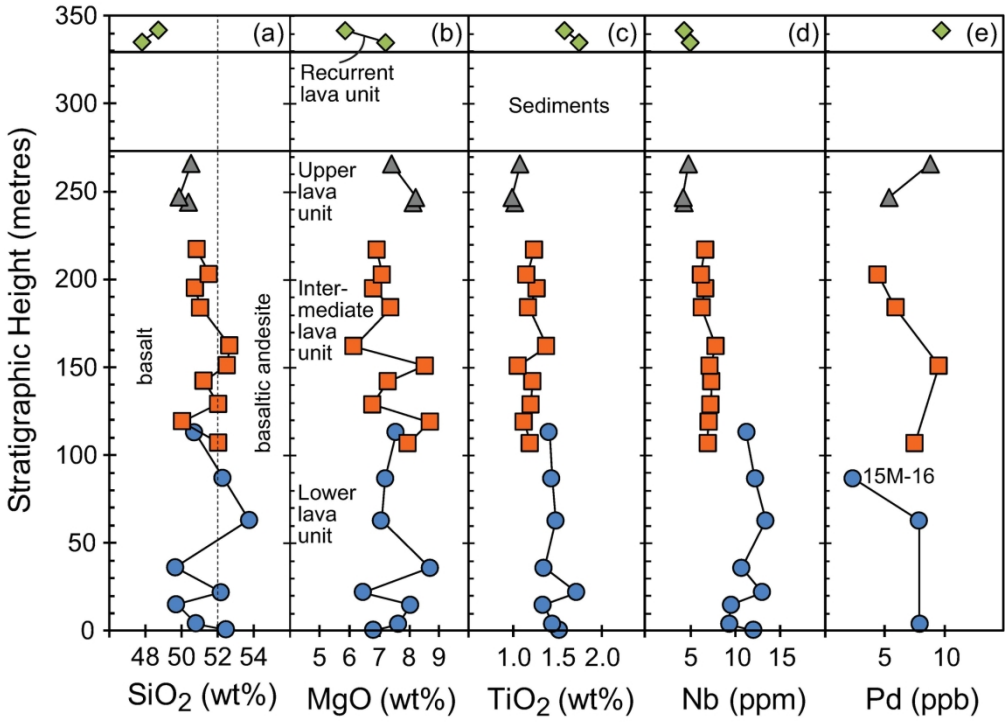

Figure 3 (Tegner et al., 2018)

Fig. 3

176x188mm (300 x 300 DPI)

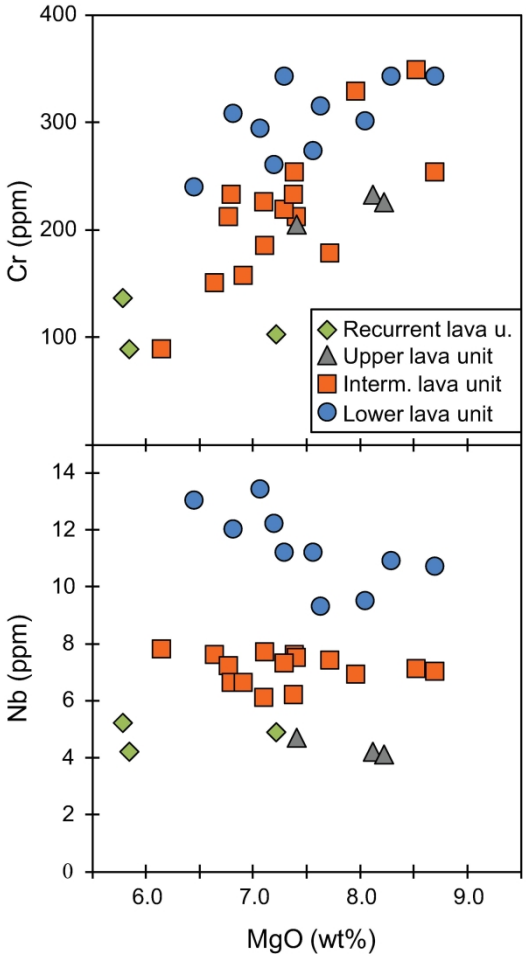

Figure 4 (Tegner et al., 2018)

Fig. 4

227x521mm (300 x 300 DPI)

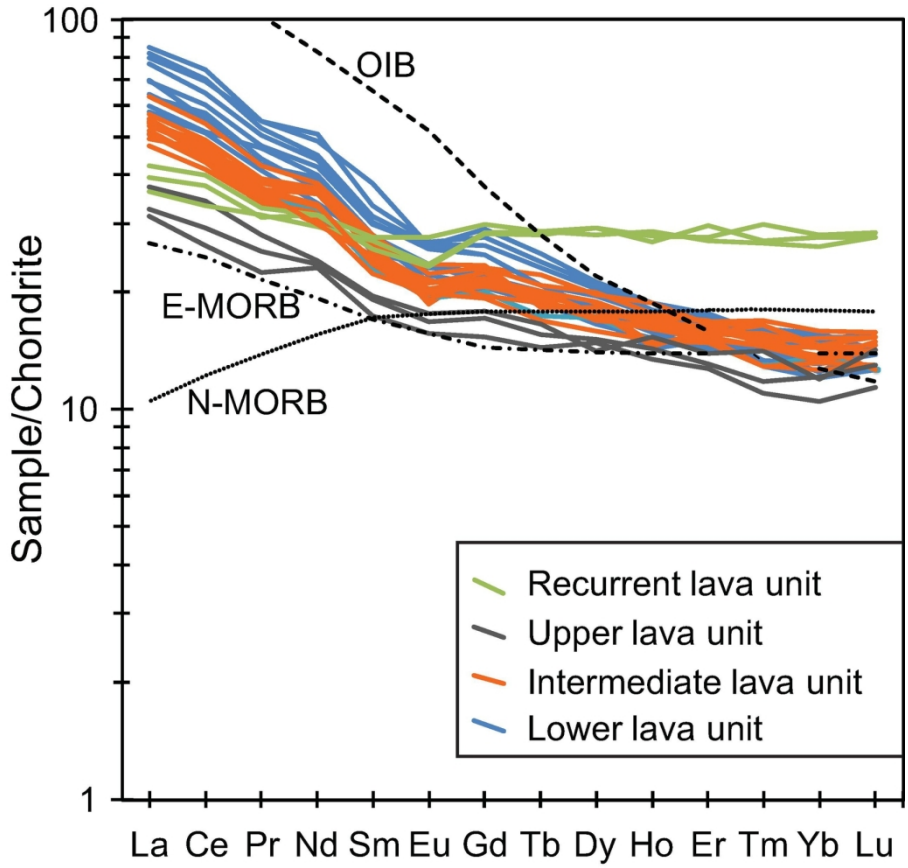

Figure 5 (Tegner et al., 2018)

Fig. 5

144x192mm (300 x 300 DPI)

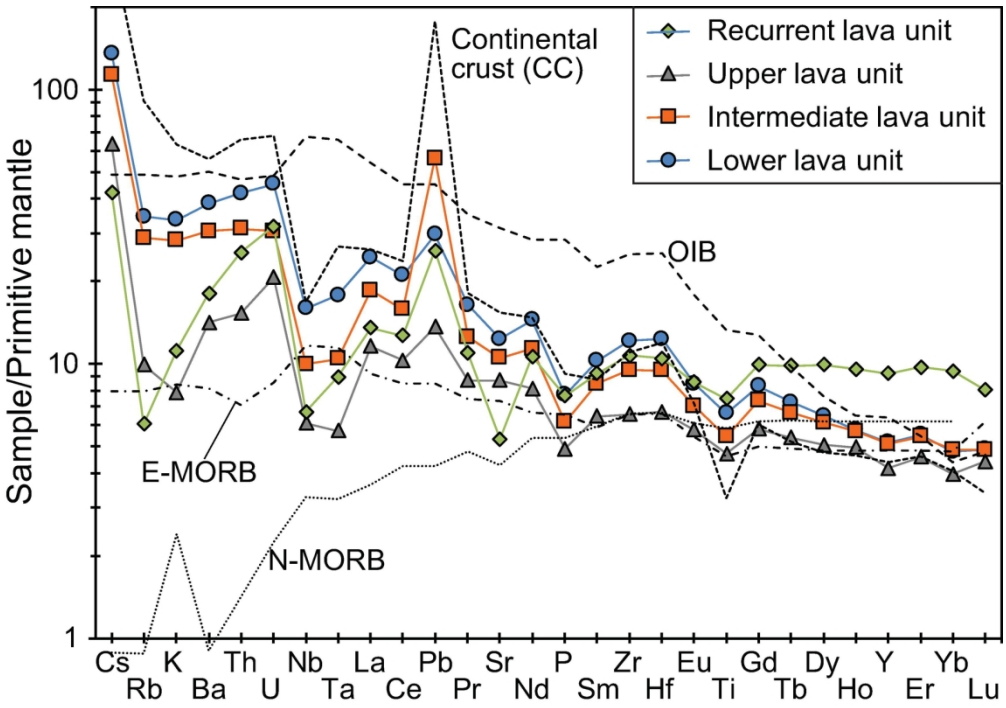

Figure 6 (Tegner et al., 2018)

Fig. 6

155x167mm (300 x 300 DPI)

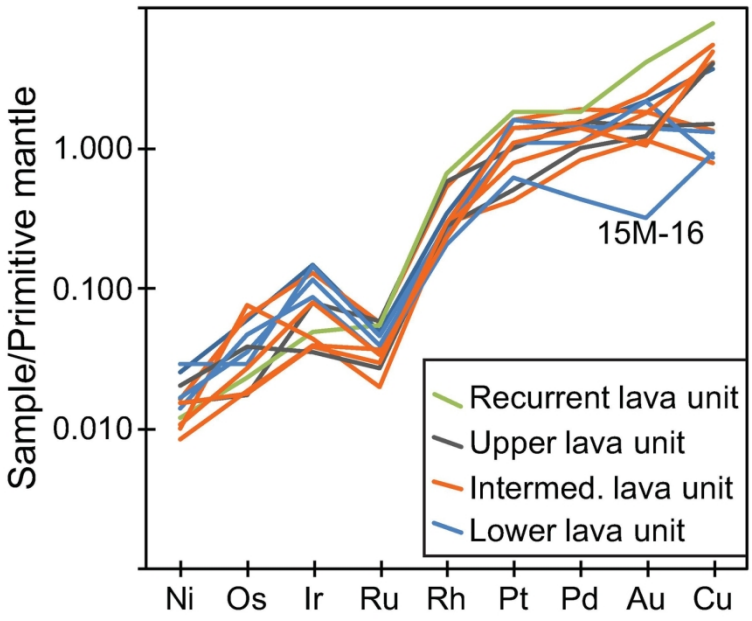

Figure 7 (Tegner et al., 2018)

Fig. 7

157x192mm (300 x 300 DPI)

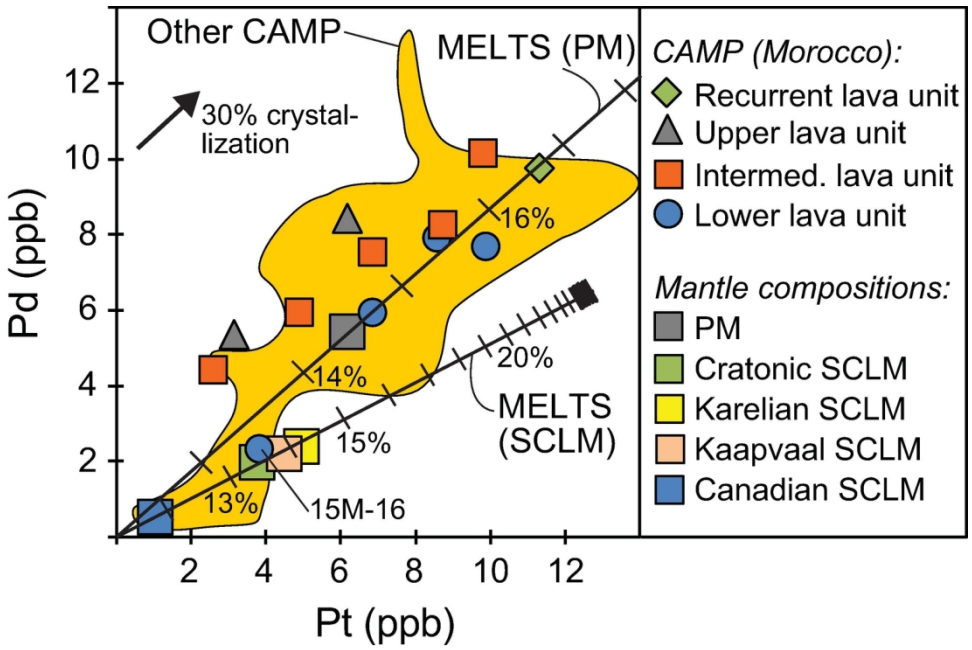

Figure 8 (Tegner et al., 2018)

Fig. 8

147x183mm (300 x 300 DPI)

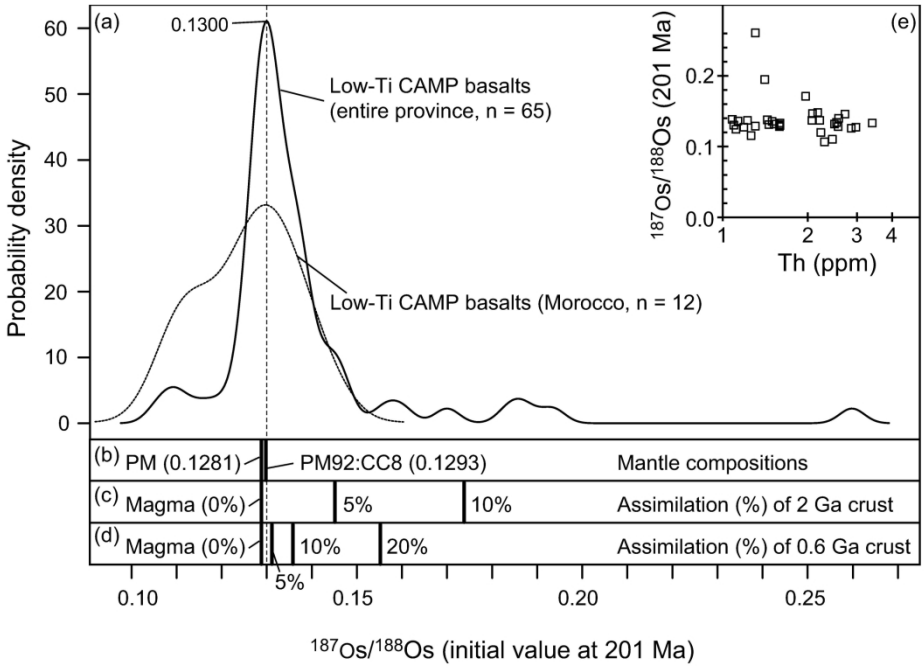

Figure 9 (Tegner et al., 2018)

Figure 9

209x236mm (300 x 300 DPI)

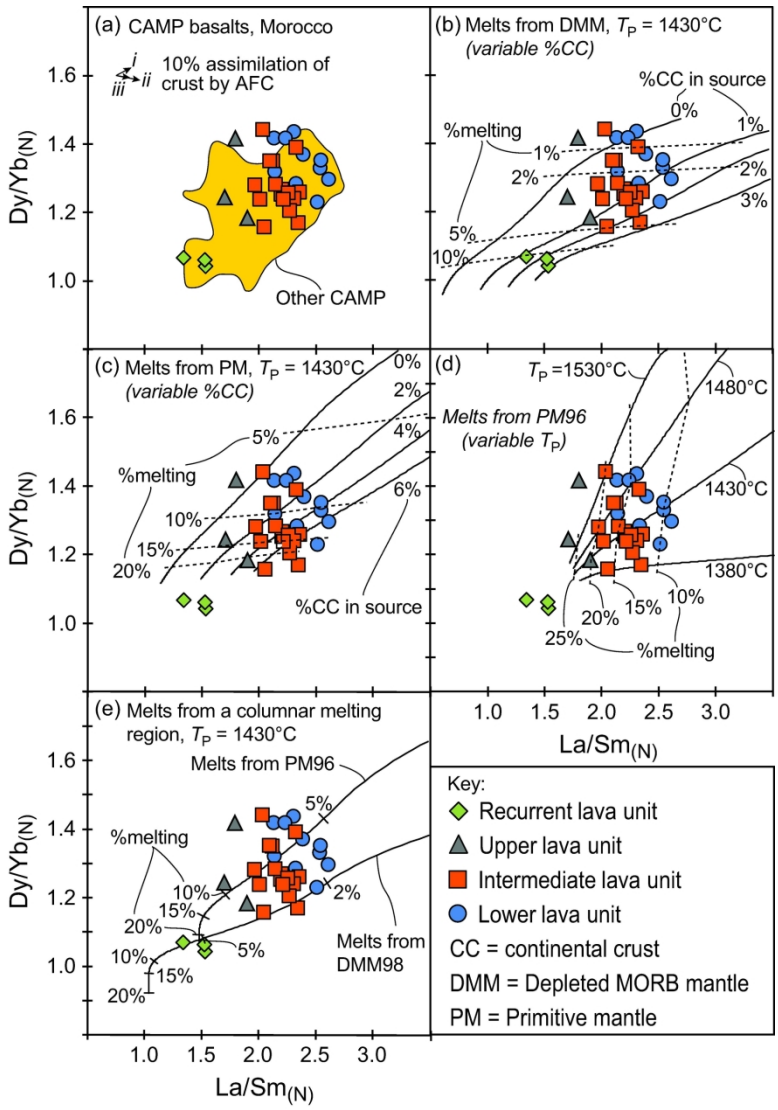

Figure 10 (Tegner et al., 2018)

Figure 10

153x238mm (300 x 300 DPI)

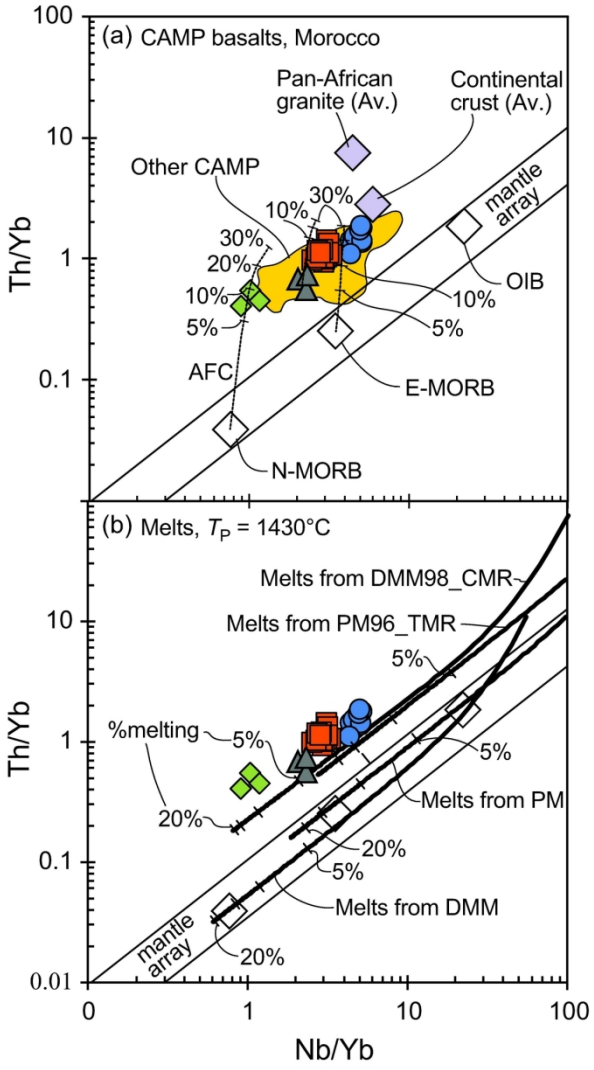

Figure 11 (Tegner et al., 2018)

Figure 11

100x204mm (300 x 300 DPI)

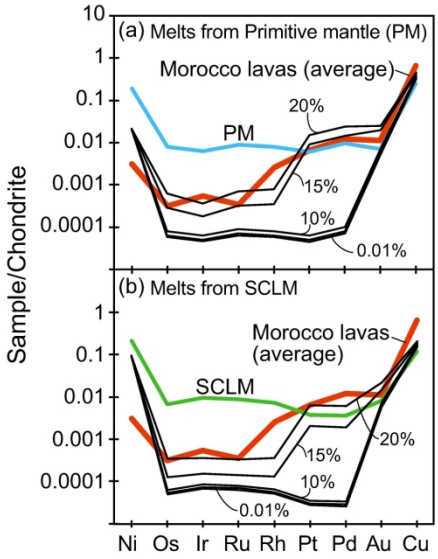

Figure 12 (Tegner et al., 2018)

Figure 12

180x238mm (300 x 300 DPI)

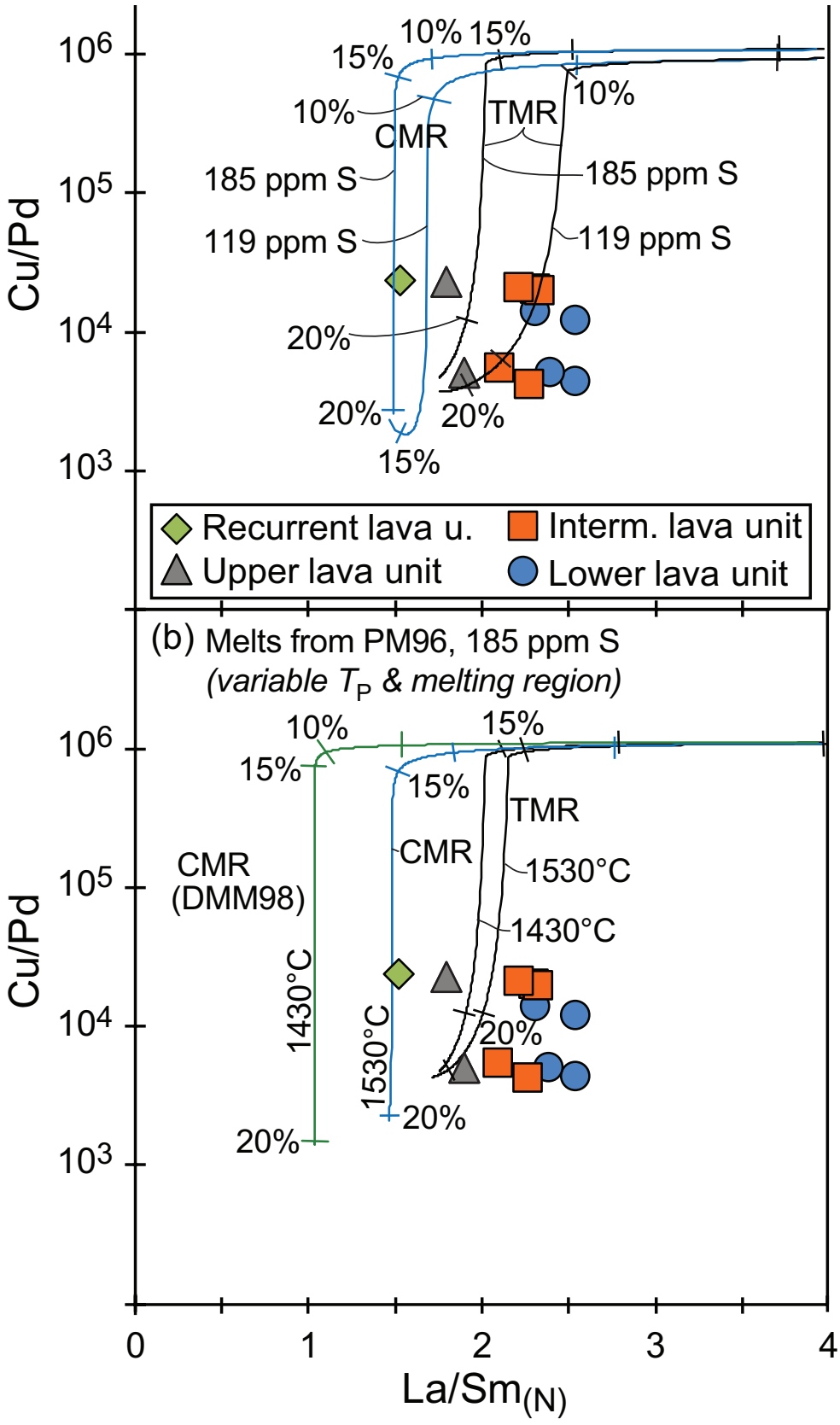

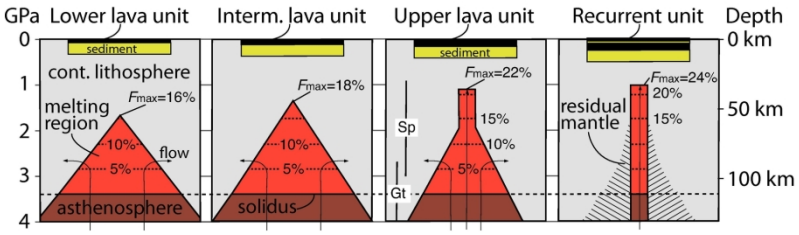

Figure 14 (Tegner et al., 2018)

Figure 14

191x155mm (300 x 300 DPI)

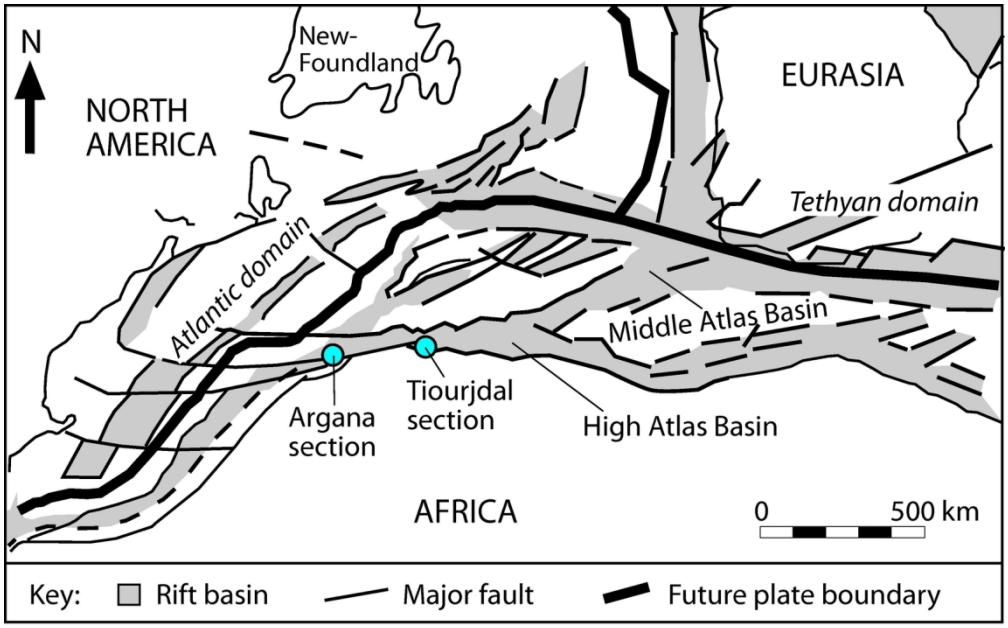

Figure 15 (Tegner et al., 2018)

Figure 15

144x135mm (300 x 300 DPI)

Table 1. Bulk rock data for CAMP flood basalts in Morocco

Sample n.			15M-05	16M-34	15M-10	15M-11	15M-12	15M-13	15M-14	15M-15	15M-16	15M-18	15M-01
Location			Argana	Argana	Tiourjdal	Tiourjdal	Tiourjdal	Tiourjdal	Tiourjdal	Tiourjdal	Tiourjdal	Tiourjdal	Argana
Lava unit			L.U.	L.U.	L.U.	L.U.	L.U.	L.U.	L.U.	L.U.	L.U.	L.U.	I.U.
Strat. height in m (Tiourjdal section)					0.5	4	15	22	36	63	87	113	
weight%	*method*	*det. limit*											
SiO2	*xrf**		51.70	51.22	52.47	50.80	49.71	52.19	49.63	53.73	52.27	50.71	51.47
TiO2	*xrf**		1.39	1.33	1.52	1.45	1.34	1.72	1.35	1.48	1.44	1.41	0.62
Al2O3	*xrf**		13.36	13.74	13.87	14.01	14.25	14.17	13.92	13.62	13.83	13.97	14.39
Fe2O3	*xrf**		9.70	10.36	10.82	10.03	10.22	10.59	9.98	10.42	10.87	11.06	10.19
MgO	*xrf**		7.29	8.29	6.81	7.63	8.05	6.45	8.70	7.07	7.20	7.56	7.39
MnO	*xrf**		0.21	0.17	0.11	0.13	0.14	0.23	0.09	0.16	0.15	0.17	0.17
CaO	*xrf**		8.04	8.35	9.20	9.22	9.43	9.29	8.12	9.14	9.41	9.59	6.08
Na2O	*xrf**		2.80	2.49	2.33	2.24	2.20	2.43	2.22	2.29	2.33	2.28	4.54
K2O	*xrf**		2.38	1.21	1.03	0.85	0.39	1.01	0.63	1.21	0.85	0.53	1.16
P2O5	*xrf**		0.16	0.15	0.20	0.15	0.14	0.20	0.16	0.20	0.16	0.16	0.14
LOI			2.29	1.88	1.49	3.31	4.10	2.02	5.33	1.24	1.48	2.89	3.29
Total			99.37	99.24	99.90	99.87	100.01	100.34	100.18	100.60	100.03	100.37	99.48
ppm													
V	*icpms**	8	290	268	281	329	309	339	292	283	313	301	319
Cr	*xrf**	7	342	342	308	315	301	239	342	294	260	274	253
Co	*icpms**	0.2	41.4	47.5	37.7	43.3	41.2	39.4	43.8	39.6	44.1	42	51.6
Ni	*icpms**	0.1	57	35	35.4	49.9	45.6	33.7	59.6	32.4	27.6	37.6	40.6
Cu	*icpms**	0.1	25.7	182.4	31.8	109.9	118.2	74	79.9	39.7	27.8	62.8	196.1
Zn	*icpms**	1	105	53	9	47	46	101	18	38	16	35	64
Ga	*icpms**	0.5	15.8	15.6	16.3	17.7	16.2	19	16.8	18.3	18	17.1	17
Rb	*icpms**	0.1	43.8	15.4	28.7	20.7	7.7	25.2	5.8	38.1	14.9	18.1	20.4
Sr	*icpms**	0.5	262.2	217.7	252.7	264.8	281.4	267.8	267	249	262.5	278.2	334.1
Y	*icpms**	0.1	21.2	23.7	24.5	20.8	19.3	25.3	23.9	26.7	25.8	23.5	24.2
Zr	*icpms**	0.1	126.8	125.4	150	122	114.4	159.8	123.1	156.7	142.3	136.3	109.3
Nb	*icpms**	0.1	11.2	10.9	12	9.3	9.5	13	10.7	13.4	12.2	11.2	7.6
Mo	*icpms**	0.1	0.5	0.5	0.2	0.3	0.3	0.5	0.1	0.3	0.1	0.2	0.3
Sn	*icpms**	1	1	<1	<1	1	1	1	<1	1	1	1	<1
Cs	*icpms**	0.1	1.1	0.6	0.9	1	1	0.9	0.3	1.3	1	2.6	0.1
Ba	*icpms**	1	516	296	264	243	171	271	223	250	241	206	195
La	*icpms**	0.1	16.5	14.2	19.4	15.2	13.7	20.1	15.0	18.9	18.2	16.4	11.2
Ce	*icpms**	0.1	33.9	31.5	43.1	33.6	31.2	45.3	35.1	42.4	39.5	36.9	25.3
Pr	*icpms**	0.02	4.00	4.44	4.98	4.04	3.90	5.21	4.16	5.21	4.79	4.51	3.23
Nd	*icpms**	0.3	18.4	18.6	20.9	18.0	15.8	22.7	17.1	23.7	20.4	19.5	15.0

*Data from package LF600, Acme Bureau Veritas Labs, Canada; #nickel fire assay pre-concentration icpms, Cardiff University, UK
Abbreviations: L.U. = lower lava unit; I.U. = intermediate lava unit; U.U. = upper lava unit; R.U. = recurrent lava unit; xrf = X-ray fluorescence; icpms = inductively coupled plasma mass spectrometry

Sample n.	15M-08	15M-02	15M-03	15M-04	15M-17	15M-19	15M-20	15M-21	15M-22	15M-23	15M-26	15M-27
Location	Argana	Argana	Argana	Argana	Tiourjdal	Tiourjdal	Tiourjdal	Tiourjdal	Tiourjdal	Tiourjdal	Tiourjdal	Tiourjdal
Lava unit	I.U.	I.U.	I.U.	I.U.	I.U.	I.U.	I.U.	I.U.	I.U.	I.U.	I.U.	I.U.
Strat. height in m (Tiourjdal section)					107	119	129	142	151	162	184	195
weight%												
SiO2	52.08	50.79	50.19	51.86	52.03	50.01	52.03	51.23	52.49	52.65	51.04	50.73
TiO2	1.23	1.35	1.28	1.28	1.19	1.13	1.20	1.22	1.06	1.38	1.18	1.27
Al2O3	14.05	14.71	13.98	13.92	13.63	13.94	14.10	14.12	13.45	14.45	14.22	14.76
Fe2O3	11.17	10.86	11.12	10.67	11.02	10.64	11.23	11.13	11.17	10.01	10.52	10.49
MgO	7.40	7.11	7.72	6.64	7.96	8.70	6.77	7.29	8.52	6.15	7.38	6.80
MnO	0.19	0.08	0.20	0.14	0.17	0.17	0.17	0.13	0.15	0.17	0.18	0.11
CaO	9.22	3.69	8.03	9.13	9.96	9.29	10.27	9.67	10.01	8.81	9.74	9.87
Na2O	1.82	5.00	3.00	2.35	2.11	1.95	2.19	2.12	1.97	2.27	2.08	2.15
K2O	1.36	1.88	1.63	1.63	0.43	0.25	0.42	0.45	0.71	0.72	0.36	0.69
P2O5	0.14	0.17	0.14	0.15	0.14	0.13	0.14	0.14	0.14	0.16	0.14	0.14
LOI	1.29	4.02	2.58	1.99	1.59	4.31	1.39	2.69	0.91	3.34	2.97	2.99
Total	99.98	99.69	99.90	99.78	100.28	100.56	99.94	100.22	100.63	100.12	99.84	100.03
ppm												
V	304	331	319	323	298	307	304	308	247	336	301	312
Cr	212	185	178	151	328	253	212	219	349	89	233	233
Co	44.9	34.5	44.8	45.7	45.7	44.9	45	44	47.8	36.9	42.4	39.3
Ni	36	49.7	34.2	29.9	21.1	33.5	27.4	32.2	32.3	20.3	19.9	34
Cu	143.6	9	131.3	165.7	148.5	114	100.4	34.5	39.8	136.6	123	30.9
Zn	125	52	103	93	36	45	31	14	12	57	48	15
Ga	15.4	13.5	16.6	17.1	14.6	17.1	16.8	15.6	14.9	16.7	16.4	17.1
Rb	37.1	20.3	20.4	37.8	13.7	4.8	17.9	17.7	20.9	19.6	7.4	12.9
Sr	224.9	239.6	267.9	218.3	184.4	218	196	199.3	176.1	211.1	217.8	216.9
Y	22.5	23.5	24.4	22.6	22.3	23.2	23.1	23.1	21.5	26.2	22.3	22.3
Zr	104.7	116.4	106.4	108.9	100.9	102.5	105	104.1	96.9	119.1	106.6	108
Nb	7.5	7.7	7.4	7.6	6.9	7	7.2	7.3	7.1	7.8	6.2	6.6
Mo	0.3	0.3	0.4	0.4	0.2	0.3	0.3	0.1	0.1	0.3	0.2	<0.1
Sn	<1	2	<1	1	<1	<1	<1	<1	<1	1	<1	<1
Cs	2.4	<0.1	0.5	1.7	1.5	1.1	1.4	1.3	0.5	0.7	0.5	0.3
Ba	201	328	474	301	163	135	174	146	156	204	184	179
La	12.9	13.5	13.2	12.9	13.0	12.0	12.9	12.9	12.0	15.0	12.6	12.9
Ce	27.4	30.1	28.2	28.0	27.5	27.1	29.3	26.5	26.3	33.1	28.6	27.5
Pr	3.44	3.71	3.50	3.48	3.31	3.33	3.48	3.41	3.19	3.99	3.44	3.58
Nd	13.9	17.3	15.4	15.6	14.8	15.3	16.7	14.6	14.3	17.7	15.4	16.3

*Data from package LF600, Acme Bureau Veritas Labs, Canada; #nickel fire assay pre-concentration icpms, Cardiff University, UK
Abbreviations: L.U. = lower lava unit; I.U. = intermediate lava unit; U.U. = upper lava unit; R.U. = recurrent lava unit; xrf = X-ray fluorescence; icpms = inductively coupled plasma mass spectrometry

Sample n.	15M-28	15M-29	15M-31	15M-32	15M-33	15M-38	15M-39	16M-03
Location	Tiourjdal	Tiourjdal	Tiourjdal	Tiourjdal	Tiourjdal	Agouim	Agouim	Ait Ourir
Lava unit	I.U.	I.U.	U.U.	U.U.	U.U.	R.U.	R.U.	R.U.
Strat. height in m (Tiourjdal section)	203	217	244	247	266	335	342	
weight%								
SiO2	51.52	50.82	50.35	49.85	50.52	47.78	48.71	48.97
TiO2	1.16	1.24	1.02	0.99	1.08	1.75	1.58	1.56
Al2O3	14.24	14.09	14.53	14.51	14.58	14.13	13.18	13.04
Fe2O3	10.90	11.31	10.72	10.59	10.94	13.64	15.91	15.58
MgO	7.10	6.91	8.12	8.22	7.40	7.21	5.84	5.78
MnO	0.14	0.12	0.16	0.17	0.16	0.38	0.24	0.30
CaO	10.12	9.71	11.73	11.71	11.63	9.66	10.10	10.02
Na2O	2.07	2.06	1.87	1.81	1.96	2.26	2.10	2.20
K2O	0.61	0.44	0.23	0.18	0.30	0.39	0.30	0.32
P2O5	0.13	0.13	0.11	0.10	0.11	0.18	0.16	0.16
LOI	1.63	3.35	1.50	2.18	1.46	2.90	2.05	1.69
Total	99.65	100.20	100.37	100.34	100.17	100.30	100.18	99.64
ppm								
V	312	297	294	288	310	473	450	442
Cr	226	157	233	226	205	103	89	137
Co	44.8	42.6	43	42.1	41.6	52.1	53.1	54.5
Ni	16.4	21.6	28.2	39.6	29.8	33.2	23.4	24.8
Cu	23.8	49.7	102.1	122.1	44.4	266.2	231.4	257.3
Zn	10	10	38	44	47	268	100	88
Ga	17	15.3	15.1	14.6	15.7	18.5	17.8	18.7
Rb	14.8	8.2	6.4	4.2	8.3	2.8	4	4.7
Sr	211.6	212.2	187.2	180.1	184.2	116	117.2	103.8
Y	23.5	23.3	20.5	17.6	18.7	41.3	42.1	42.5
Zr	103.7	102.6	72	67.5	80.5	127.4	116.7	115.9
Nb	6.1	6.6	4.2	4.1	4.7	4.9	4.2	5.2
Mo	0.1	<0.1	0.2	0.2	0.1	0.6	0.6	0.5
Sn	1	<1	<1	<1	<1	<1	<1	1
Cs	0.8	0.5	0.6	0.6	0.3	0.2	0.3	0.5
Ba	178	168	116	78	102	126	124	128
La	12.3	11.7	7.7	7.4	8.8	10.0	9.3	8.6
Ce	26.6	28.4	17.8	16.1	20.9	24.3	22.9	20.4
Pr	3.31	3.37	2.42	2.13	2.66	3.11	2.95	2.99
Nd	13.9	14.2	11.0	10.8	11.2	14.7	14.7	13.7

*Data from package LF600, Acme Bureau Veritas Labs, Canada; #nickel fire assay pre-concentration icpms, Cardiff University, UK
Abbreviations: L.U. = lower lava unit; I.U. = intermediate lava unit; U.U. = upper lava unit; R.U. = recurrent lava unit; xrf = X-ray fluorescence; icpms = inductively coupled plasma mass spectrometry

ppm			15M-05	16M-34	15M-10	15M-11	15M-12	15M-13	15M-14	15M-15	15M-16	15M-18	15M-01
Sm	*icpms**	0.05	4.19	4.28	4.79	4.25	4.14	5.80	3.85	5.10	4.62	4.55	3.67
Eu	*icpms**	0.02	1.23	1.34	1.54	1.37	1.28	1.53	1.35	1.56	1.49	1.53	1.15
Gd	*icpms**	0.05	4.48	4.64	5.40	4.34	4.28	5.96	4.46	5.69	5.12	5.13	4.34
Tb	*icpms**	0.01	0.75	0.70	0.86	0.70	0.69	0.94	0.75	0.89	0.78	0.78	0.73
Dy	*icpms**	0.05	4.53	4.20	5.17	4.55	4.34	5.40	4.52	5.32	4.97	4.61	4.65
Ho	*icpms**	0.02	0.89	0.86	1.01	0.89	0.81	1.06	0.96	1.02	0.99	0.92	0.97
Er	*icpms**	0.03	2.55	2.38	2.86	2.36	2.49	2.92	2.77	2.79	2.75	2.55	2.59
Tm	*icpms**	0.01	0.33	0.34	0.41	0.36	0.33	0.40	0.39	0.40	0.38	0.36	0.42
Yb	*icpms**	0.05	2.28	2.13	2.67	2.12	2.05	2.55	2.46	2.60	2.46	2.22	2.43
Lu	*icpms**	0.01	0.37	0.33	0.36	0.37	0.32	0.40	0.36	0.39	0.36	0.35	0.35
Hf	*icpms**	0.1	3.7	3.5	4.2	3.5	3.1	4.5	3.6	4.5	3.9	3.5	2.6
Ta	*icpms**	0.1	0.7	0.7	0.8	0.6	0.5	1.0	0.8	0.7	0.8	0.7	0.5
W	*icpms**	0.5	0.5	0.6	0.6	0.9	<0.5	0.6	<0.5	0.6	0.8	<0.5	<0.5
Pb	*icpms**	0.1	10	2.2	1.1	0.6	1.5	1.2	0.8	0.9	1.4	1.3	20.2
Th	*icpms**	0.2	3.8	2.9	3.5	3.0	3.1	3.6	2.7	4.6	4.2	4.1	2.9
U	*icpms**	0.1	1.1	0.7	0.9	0.8	0.8	1.0	0.9	1.1	1.0	1.2	0.4
ppb													
Au	*icpms#*		2.20			2.19				1.33	0.32		
Pd	*icpms#*		5.91			7.91				7.86	2.33		
Pt	*icpms#*		6.86			8.59				9.82	3.84		
Rh	*icpms#*		0.29			0.35				0.30	0.21		
Ru	*icpms#*		0.29			0.31				0.26	0.21		
Ir	*icpms#*		0.42			0.43				0.35	0.25		
Os	*icpms#*		0.11			0.23				0.15	0.18		

*Data from package LF600, Acme Bureau Veritas Labs, Canada; #nickel fire assay pre-concentration icpms, Cardiff University, UK
Abbreviations: L.U. = lower lava unit; I.U. = intermediate lava unit; U.U. = upper lava unit; R.U. = recurrent lava unit; xrf = X-ray fluorescence; icpms = inductively coupled plasma mass spectrometry

ppm	15M-08	15M-02	15M-03	15M-04	15M-17	15M-17	15M-20	15M-21	15M-22	15M-23	15M-26	15M-27	15M-28	15M-29
Sm	3.78	4.10	3.61	3.61	3.60	3.52	3.88	3.55	3.41	4.29	3.67	4.06	3.78	3.75
Eu	1.16	1.08	1.22	1.11	1.14	1.12	1.22	1.18	1.15	1.29	1.25	1.25	1.18	1.16
Gd	4.25	4.73	4.44	4.41	4.20	4.09	4.60	4.29	3.96	4.73	4.01	4.75	4.39	4.41
Tb	0.72	0.83	0.73	0.75	0.70	0.65	0.71	0.72	0.63	0.78	0.70	0.69	0.69	0.70
Dy	4.28	5.00	4.61	4.80	4.26	4.36	4.37	4.35	4.03	5.07	4.55	4.27	4.54	4.31
Ho	0.93	1.06	0.98	0.95	0.92	0.85	0.99	0.89	0.85	1.00	0.94	0.92	0.82	0.91
Er	2.53	2.74	2.80	2.71	2.60	2.49	2.59	2.64	2.45	2.78	2.60	2.44	2.64	2.50
Tm	0.37	0.42	0.37	0.38	0.34	0.33	0.39	0.35	0.33	0.43	0.40	0.38	0.38	0.37
Yb	2.26	2.48	2.45	2.59	2.22	2.33	2.28	2.49	2.24	2.70	2.46	2.47	2.25	2.33
Lu	0.38	0.39	0.37	0.39	0.36	0.32	0.38	0.33	0.33	0.40	0.32	0.33	0.36	0.36
Hf	2.7	3.2	2.9	3.0	3.0	2.8	3.0	2.8	2.7	3.3	2.9	3.0	3.1	2.7
Ta	0.5	0.6	0.6	0.5	0.5	0.3	0.5	0.4	0.3	0.4	0.4	0.4	0.3	0.2
W	<0.5	<0.5	<0.5	0.7	<0.5	<0.5	<0.5	<0.5	<0.5	<0.5	<0.5	<0.5	<0.5	<0.5
Pb	1.2	5.3	2.6	19.9	0.9	0.6	0.6	2.1	0.8	1.2	1	1.5	1.1	0.8
Th	2.4	3.5	2.5	2.4	2.3	2.3	3.0	2.5	2.5	3.2	2.4	2.5	2.6	2.6
U	0.6	0.8	0.5	0.6	0.9	0.5	0.8	0.8	0.6	0.6	0.6	0.7	0.6	0.6
ppb														
Au				2.44	1.05				1.83		1.77		1.14	
Pd				8.25	7.51				9.52		5.90		4.40	
Pt				8.74	6.87				9.34		4.92		2.64	
Rh				0.30	0.24				0.57		0.29		0.30	
Ru				0.18	0.21				0.35		0.13		0.23	
Ir				0.11	0.23				0.35		0.13		0.11	
Os				0.07	0.11				0.22		0.30		0.07	

*Data from package LF600, Acme Bureau Veritas Labs, Canada; #nickel fire assay pre-concentration icpms, Cardiff University, UK
Abbreviations: L.U. = lower lava unit; I.U. = intermediate lava unit; U.U. = upper lava unit; R.U. = recurrent lava unit; xrf = X-ray fluorescence; icpms = inductively coupled plasma mass spectrometry

ppm	15M-31	15M-32	15M-33	15M-38	15M-39	16M-03
Sm	2.92	2.66	2.99	4.21	3.94	4.14
Eu	0.97	0.91	1.02	1.60	1.35	1.37
Gd	3.53	3.16	3.67	6.14	5.78	5.84
Tb	0.58	0.54	0.62	1.07	1.05	1.07
Dy	3.83	3.77	3.59	7.43	7.43	7.09
Ho	0.81	0.76	0.87	1.57	1.52	1.62
Er	2.17	2.10	2.30	4.58	4.90	4.49
Tm	0.30	0.28	0.36	0.76	0.69	0.68
Yb	2.06	1.78	2.03	4.77	4.68	4.44
Lu	0.33	0.29	0.36	0.72	0.70	0.70
Hf	2.3	1.7	2.2	3.4	3.1	3.2
Ta	0.2	0.3	0.2	0.4	0.3	0.4
W	<0.5	<0.5	<0.5	<0.5	<0.5	<0.5
Pb	1.1	0.7	1.1	2.5	1	2
Th	1.4	1.0	1.5	2.6	1.9	2.0
U	0.4	0.4	0.5	0.9	0.6	0.5
ppb						
Au		1.22	1.42		4.13	
Pd		5.36	8.81		9.75	
Pt		3.16	6.43		11.32	
Rh		0.29	0.66		0.68	
Ru		0.17	0.36		0.35	
Ir		0.10	0.22		0.14	
Os		0.15	0.07		0.09	

*Data from package LF600, Acme Bureau Veritas Labs, Canada; #nickel fire assay pre-concentration icpms, Cardiff University, UK
Abbreviations: L.U. = lower lava unit; I.U. = intermediate lava unit; U.U. = upper lava unit; R.U. = recurrent lava unit; xrf = X-ray fluorescence; icpms = inductively coupled plasma mass spectrometry

Table 2. Summary of PGE, Au, Ni and Cu compositions and partition coefficients used in mantle melting models

Element	Unit	PM	ref	SCLM	ref.	Dsulphide/melt	ref.	Dsilicate/melt	ref.
S	ppm	119 or 185	(1,5)	119	(1)	-		-	
Ni	ppm	1960	(1)	2227	(3)	250	(4)	9	(5)
Os	ppb	3.9	(2)	3.3	(3)	400000	(5)	2	(5)
Ir	ppb	2.9	(2)	4.3	(3)	400000	(5)	3	(5)
Ru	ppb	6.3	(2)	6.3	(3)	400000	(5)	1.5	(5)
Rh	ppb	1.03	(2)	0.93	(3)	400000	(5)	1.5	(5)
Pt	ppb	6.2	(2)	3.8	(3)	400000	(5)	0.012	(5)
Pd	ppb	5.38	(2)	1.9	(3)	400000	(5)	0.012	(5)
Au	ppb	1	(1)	1.1	(3)	4000	(5)	0.002	(6)
Cu	ppm	30	(1)	14.3	(3)	1500	(5)	0.26	(5)

Abbreviations: PM = primitive mantle; SCLM = sub-continental lithospheric mantle

(1) Salters and Stracke (2004)

(2) Barnes et al. (2015)

(3) Xenoliths from cratons; average composition of 431 xenoliths compiled by Barnes et al. (2015)

(4) Rehkämper et al. (1999)

(5) Mungall and Brenan (2014); Brenan et al. (2005)

(6) Brenan et al. (2003)